Chapter 3

Matched Wavelet based Protection of Power Transformers

3.1 Outline

Studies show that wavelets have been used in the area of differential protection of power transformers. Several standard orthogonal wavelets (such as Daubechies, Meyer, Symlet, Coiflet), Bi-orthogonal wavelets (such as B-Spline), and nonorthogonal wavelets (such as Gaussian, Mexican Hat, Morlet) have been used for the purpose of differential protection. These wavelets from different wavelet families are classified according to their basis function characteristics. However, the selection of mother wavelets were done by trial and error and there is no particular reason specified for using a particular wavelet. In the present work, wavelet basis functions which optimally match with the pattern of differential current waveforms are developed. The transform of signal with matched wavelet gives the maximum energy peaks when similar pattern is met.

This chapter describes various operating conditions of the transformer along with the system model designed for the test cases. Also, the developed matched wavelet leading to modified differential protection scheme is discussed. The performance of designed matched wavelet on various test cases are studied.

The chapter has two major parts. The first part (section 3.2) contains several subsections which describe the various operating conditions and system models utilized in this work. This section also discusses the conditions such as, inrush, external fault, in-zone fault, inter-turn fault, and CT saturation in detail. The existing scheme for detection of

inrush and fault conditions are also discussed in the first part in section 3.3.1. The second part starts with the modified differential protection scheme utilizing matched wavelets and is one of the contributions of this work. This chapter also discusses the performance of matched wavelet protection scheme on various test cases. Determination of threshold for the matched inrush and matched fault wavelet is explained in section 3.3.3. Performance of the matched inrush- and fault-filter is discussed in section 3.4. The highlights of the finding of this chapter are summarized in section 3.5.

3.2 System Model and Description

To test the performance of the proposed method, experimental set-ups were designed to cover the range and its aspects as follows.

Fig. 3.1 describes the operation of a transformer in the context of differential protection. During normal operation, the differential current observed is negligible. However, during the in-zone (within the protected zone)/internal fault, the differential current is quite high. This high current serves as a signal for detecting fault in the zone under consideration. If high differential current is detected, the transformer is disconnected early from the circuit, this disconnection can restrict the time for which the fault current flows into the transformer thereby saving the transformer from damage.

When unloaded or loaded transformer is energized, high current of transient nature is drawn from the source, which is known as magnetizing inrush current, due to which core gets saturated. Thus, the differential current is also high during the energisation. This creates ambiguity in detection of in-zone fault. Apart from inrush and in-zone fault as discussion above, there are other conditions as well which give rise to further ambiguity in correct detection of inrush and in-zone fault. The detailed description of various cases which occur during operation of a transformer and which have to be taken care of in the differential protection are discussed in the following sections.

3.2.1 Magnetizing Inrush

Whenever a transformer is switched on with or without load across its secondary windings, the primary side of the transformer draws a high transient current of a typical shape from the primary side. This current is called magnetizing inrush current. The magnitude of

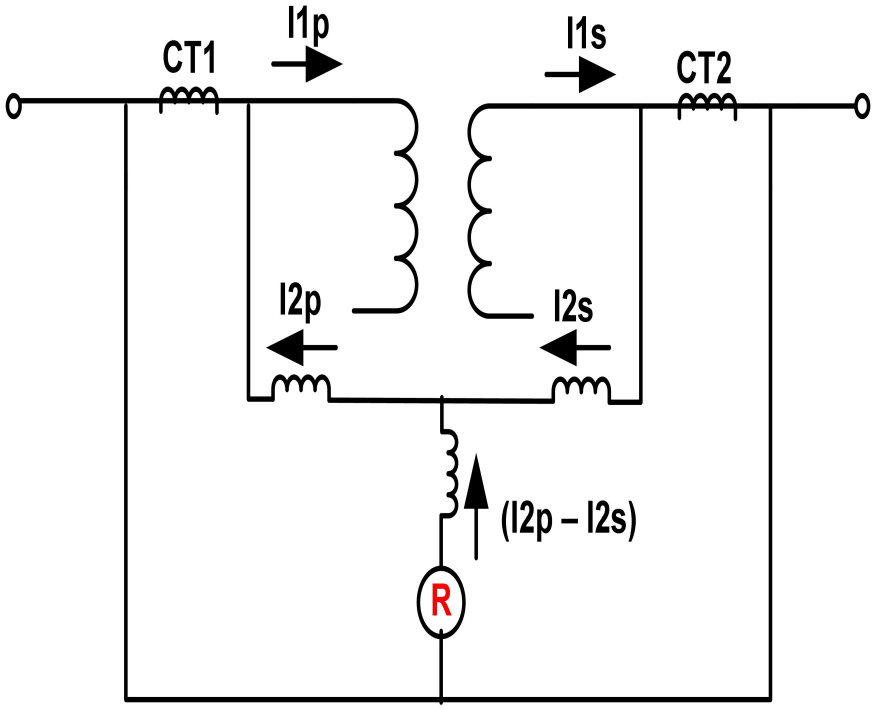

Figure 3.1: Differential protection of transformer

inrush current could be 10-15 times the normal load current and can last up to 1-2 seconds in certain cases. The time for which the inrush persist depends on the inductance (time constant) of the transformer. Inrush current may cause tripping of relays of transformer at the time of charging of the transformer which is undesirable.

Inrush current phenomena happens in devices where magnetic cores are involved. A sinusoidal voltage is impressed upon the primary winding when the transformer is switched on. In steady state conditions, the induced flux in the core is proportional to the magnetizing current and is in quadrature with the applied voltage. The relationship between the flux and the primary voltage for steady state conditions is shown in Fig. 3.2. From Fig. 3.2 it is observed that in case of steady state, the value of the flux at time t=0 is ϕ_m. With this background the typical shape of inrush along-with the equivalent circuit of transformer is explained with the help of Figs. 3.3 and 3.4. The circuit elements are defined in the figure itself.

For making calculation simple, R_C is used as combined resistance for R_1 (source resistance) and R_T (transformer resistance). Similarly, X_C is the combined reactance for X_1 (source reactance) and X_T (transformer reactance).

For calculation of inrush current, the first cycle peak of the differential current is consid-

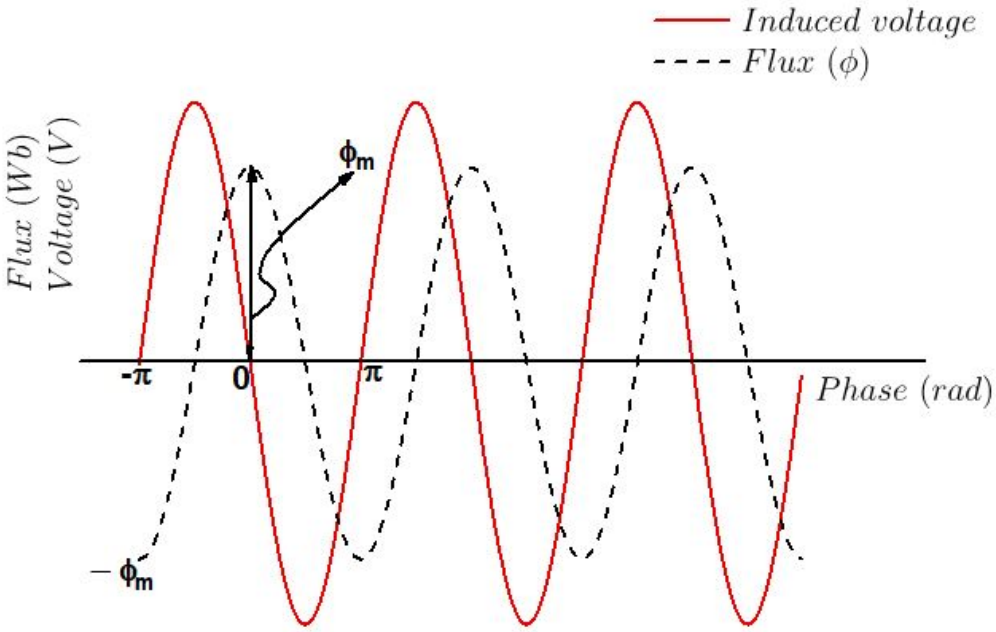

Figure 3.2: Flux produced in the core is in quadrature with applied voltage

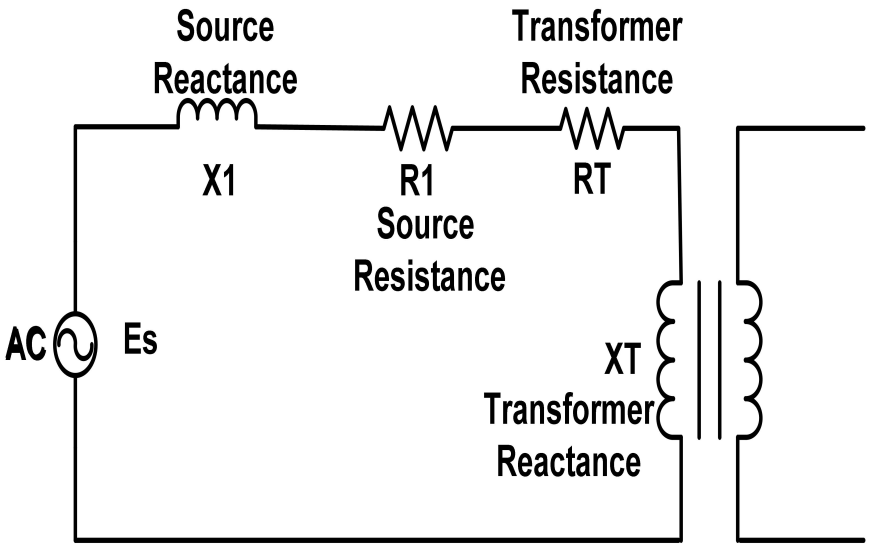

Figure 3.3: Transformer circuit

ered. For the first cycle, value of integral $\int_{\frac{-\pi}{\omega}}^{t} iR_C dt$ in the equation A.5 (see Appendix I) is negligibly small. Therefore, equation (A.5) becomes,

$$\phi = \phi_r + \phi_m(1 + cos\omega t) \tag{3.1}$$

Putting $\omega t = \pi$ in equation (3.1), it gives,

$$\phi = \phi_r. \tag{3.2}$$

Putting $\omega t = 0$ in equation (3.1), it gives,

$$\phi = \phi_r + 2\phi_m. \tag{3.3}$$

Fig. 3.4 shows the relationship between the primary voltage and the core flux in the transformer. From Fig. 3.4, it can be observed that the value of flux ϕ, at the end of first half cycle of voltage wave is $2\phi_m + \phi_r$, where ϕ_m is the maximum value of the steady state flux as shown in Fig. 3.4.

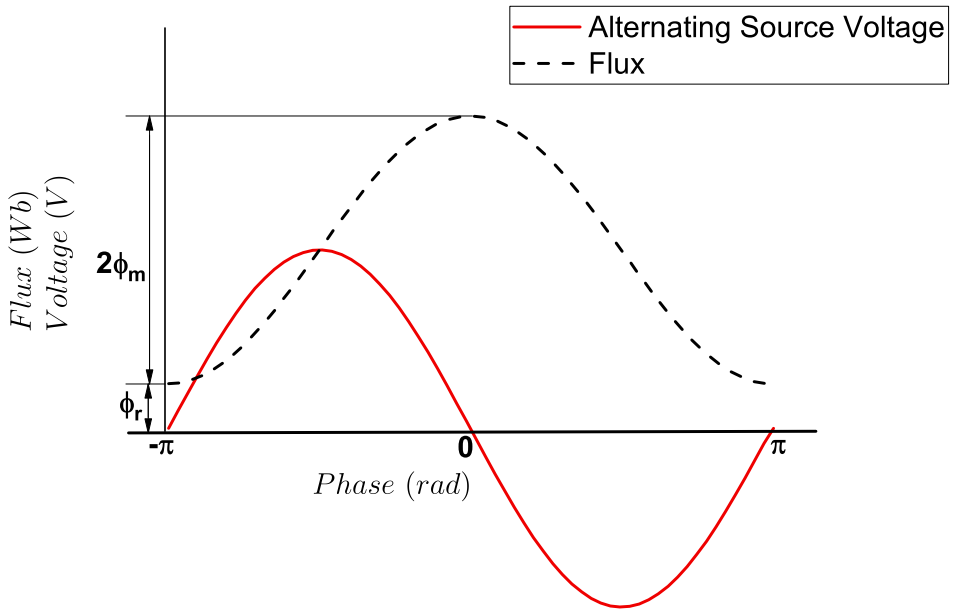

Figure 3.4: Primary voltage and flux for one cycle of operation

The core of the transformer is so made that it becomes saturated when flux reaches just above the maximum value of the steady state flux. The high current required to produce rest of the flux above ϕ_m is drawn from the primary supply. Fig 3.5 shows the effect of saturation characteristics of the transformer core on the current drawn from the primary side vis-a-vis the core flux induced in the transformer core. From Fig. 3.5, it is observed that the magnetizing inrush current is high with peaks and is unipolar in nature.

Fig. 3.6 shows PSCAD/EMTDC simulation set-up to simulate magnetizing inrush current for a transformer. In Fig. 3.6, the differential currents are simulated as difference

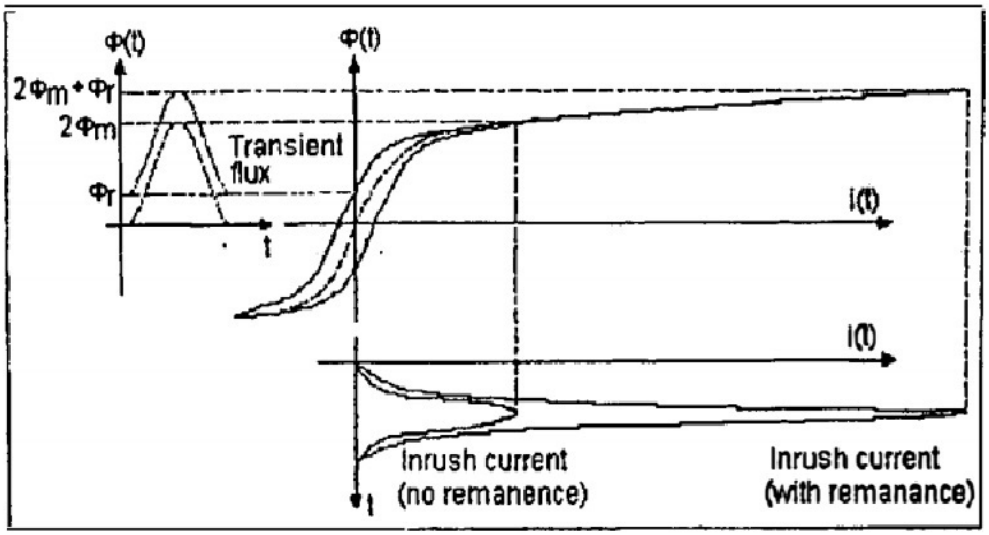

Figure 3.5: Inrush current phenomena [4]

of primary currents (I_{a1}, I_{b1}, I_{c1}) and secondary currents (I_{a2}, I_{b2}, I_{c2}). The transformer turn ratio is considered as $\frac{1}{2}$.

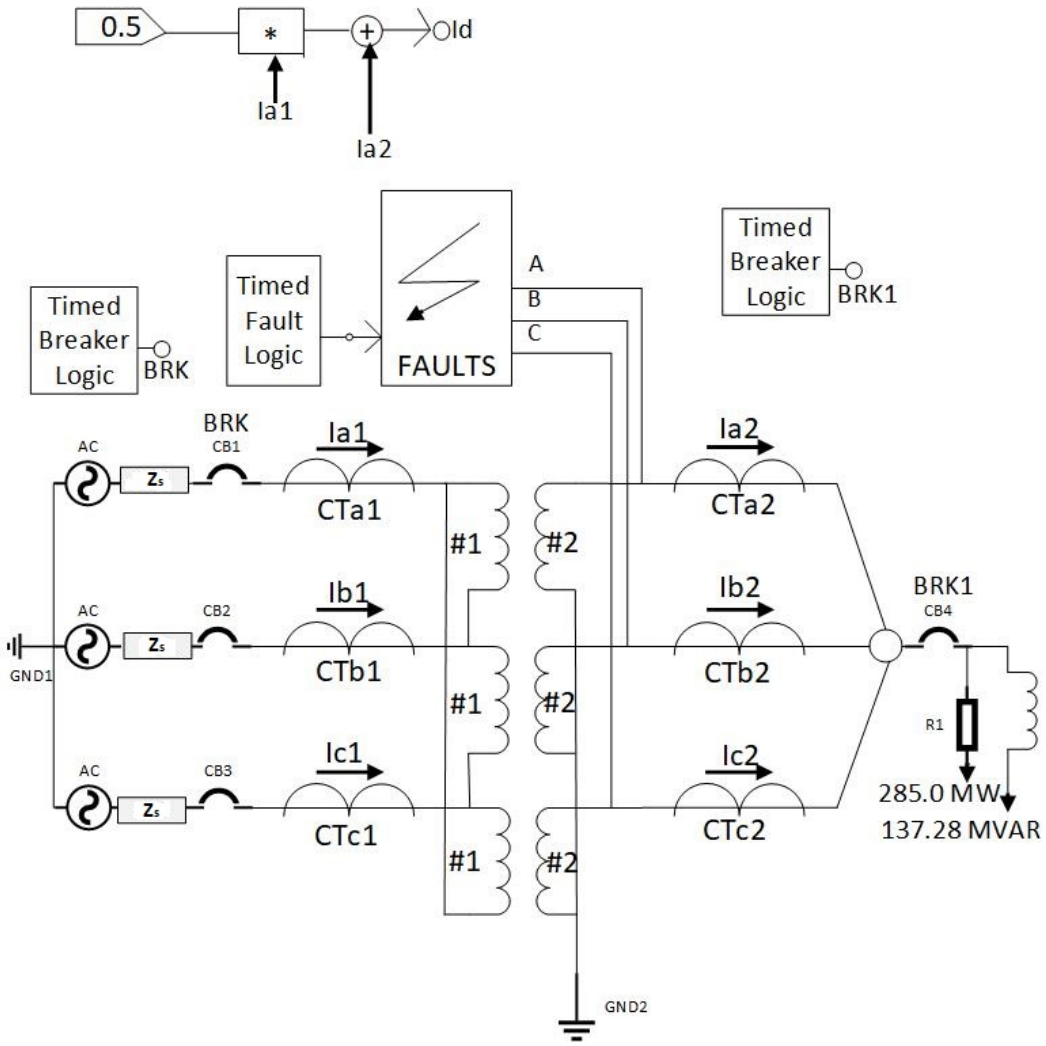

Figure 3.6: Test system for inrush and in-zone faults (source impedance $Zs = 0.0318\angle -88.1759$)

Over-fluxing

In the transformer the induced e.m.f is caused by constantly varying magnetic flux that links the two windings. The magnetic flux density in the windings are directly proportional to induced voltage and inversely proportional to the frequency.

$$B \propto \frac{V}{f} \tag{3.4}$$

Transformers are designed in such a manner that during normal operating conditions the flux density in the core is maintained just below the knee point of the saturation curve or within the linear region of the saturation curve. Over-fluxing is a phenomena when the flux density in the core increases to high levels, or significantly above the knee point of the saturation curve. The phenomenon of over-fluxing may happen due several reasons such

as, high residual flux in the core, low frequency or dc currents in the primary winding and primary winding excited at higher voltage than the rated. The over-fluxing becomes an important consideration, especially when it is coupled with inrush phenomenon. Due to over-fluxing, the magnetizing current in the primary winding of the transformer increases to high values. Under these conditions the linear relationship between primary and secondary currents does not prevail. So there may not be sufficient and appropriate reflection of this high primary magnetizing current in the secondary circuit due to which mismatch of primary current and secondary currents is likely to occur, causing differential relay to operate. Fig. 3.7 shows PSCAD/EMTDC set-up to simulate the over-fluxing phenomena in the transformer. To simulate the remnant flux the DC currents $I_{DC1}, I_{DC2}, I_{DC3}$ are injected into the transformer prior to switching on the primary side. The currents are raised from 0% to 100% of the peak flux linkages.

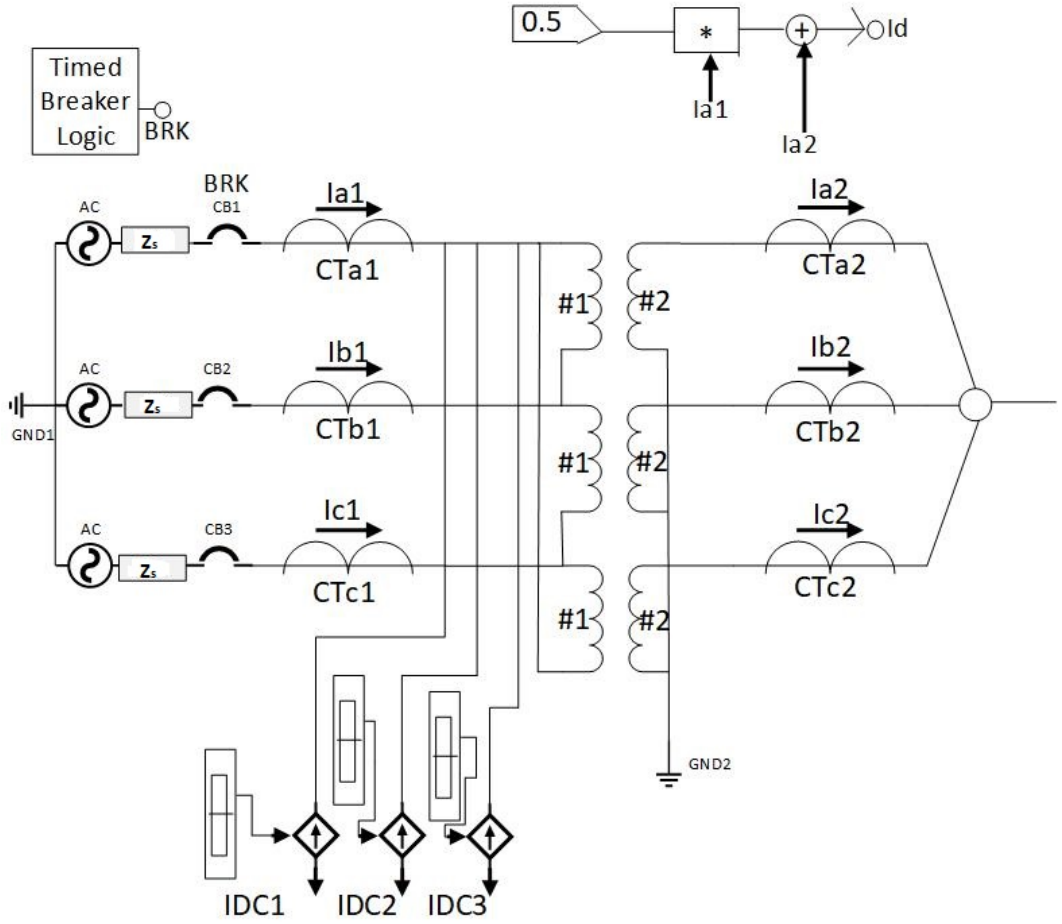

Figure 3.7: Test system for generating over-excitation condition (source impedance $Zs = 0.0318\angle - 88.1759$)

Sympathetic Inrush

Sympathetic inrush is a phenomenon where a transformer that is previously energized will exhibit a sudden change in current when a nearby unloaded or loaded transformer is switched on or energized. Sympathetic inrush is triggered by the voltage drop across the system impedance due to magnetizing inrush of the another transformer being energized. The sympathetic inrush phenomenon occurs in the transformers connected in parallel as well as in series. The authors of [83] have commented regarding sympathetic inrush in case of series connected transformers as follows.

"The results suggest that the interaction between series transformers is more than somewhat similar to the interaction occurring between the transformers in parallel previously discussed."

To verify the above fact, in the present studies, sympathetic inrush waveforms for series and parallel connected transformers were compared. It was found that the two waveforms were quite similar in nature. Since the sympathetic inrush phenomenon gives similar results for both, parallel and series connected transformers, in the present study, series connected transformers were adopted to cover various possibilities of sympathetic inrush conditions.

Mal-operation resulting from sympathetic inrush is difficult to detect, since it is not directly related to the energizing the protected transformer. Sympathetic inrush also has a high second harmonic content as in case of general magnetizing inrush. Sympathetic inrush decays more slowly than that in a single transformer configuration. A PSCAD/EMTDC simulation environment which was set-up to simulate different sympathetic inrush currents is shown in Fig. 3.8. The figure shows that out of two transformers A and B, the transformer A is already in operation and the transformer B is energized by closing the circuit breakers (BRK1). Due to this an inrush is established in the primary of transformer B, and this inrush current has a dc component. The current of already energized transformer A get an additional surge due to this inrush current and results in an asymmetrical current that is very low in harmonic content.

3.2.2 Faults in Power Transformers

Fault conditions in a transformer can be broadly categorized in following manner.

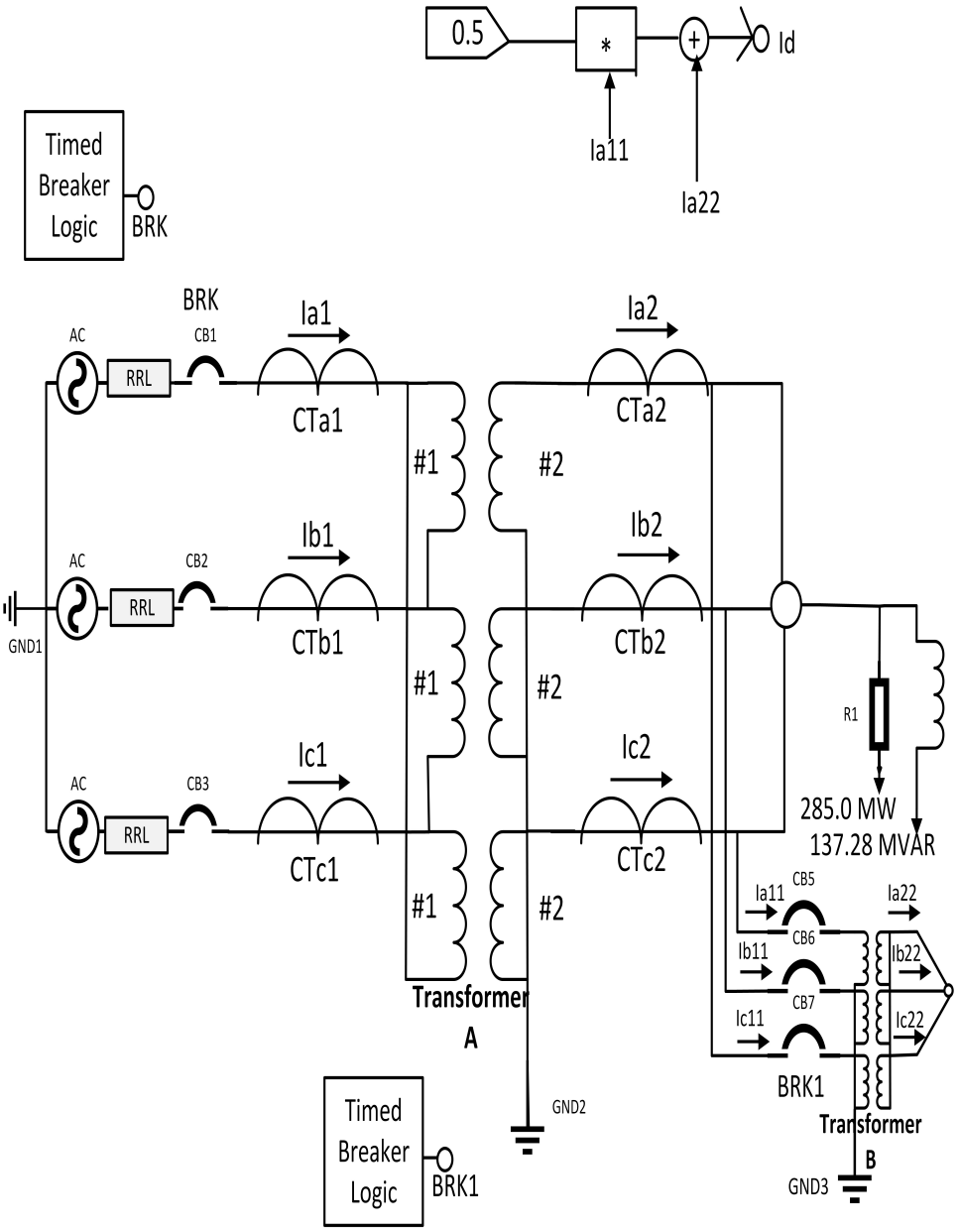

Figure 3.8: Test system for generating sympathetic inrush current (source impedance $Zs = 0.0318\angle - 88.1759$)

1. External or through fault: External faults are mainly caused due to factors such as, overloading, system faults, over voltages, and under frequency operation. External faults happens outside the differential protection zone of the transformer. Any such damage due to lightening strikes or other factors from outside is unpredictable and are taken care of by line relays. The trip of differential relays are not desirable in external faults. However, in certain cases the external faults may generate a large transient current having similar characteristics as to that of faults. The

PSCAD/EMTDC simulation circuit for external faults is given in Fig. 3.9.

2. Internal/in-zone faults: Internal faults and the in-zone faults are mostly caused due to factors such as, insulation deterioration, winding failure, overheating, and contamination of oil. Internal faults and in-zone (inside the protected zone) faults which are serious in nature, can cause immediate damage to the transformer. Since the fault is inside the protected zone, current flows only in the source side CT. These faults are detectable by imbalance of current which reflects in the differential currents. In the present context the internal faults and the in-zone faults are discriminated in the following way. The in-zone faults are the faults which occur in the protective zone whereas, the internal faults are which appears in the windings as inter-turn faults. Internal/in-zone faults can be of following types.
   (i) Phase-to-phase and phase-to-earth faults at the high voltage and low voltage terminals.
   (ii) Phase-to-phase and phase-to-earth faults at the high voltage and low voltage windings.
   (iii) Inter-turn faults occur due to winding flash over caused by line surges. A short circuit of a few turns of the winding will give rise to high currents in the short-circuited loops, but the terminal current will be low.

A simulation environment to obtain differential waveforms under different in-zone fault conditions is shown in Fig. 3.10. Fig. 3.11 depicts the PSCAD/EMTDC circuit for internal faults. The various faults simulated for testing the proposed methods are (i) Line to Ground (L-G), (ii) Line to Line (L-L), (iii) Three phase to Ground (L-L-L-G) and (iv) Three phase (L-L-L) Faults. In Fig. 3.10 by using timing logic feature of PSCAD/EMTDC the fault block and CBs were activated to generate fault at different switching angles.

3.2.3 CT Saturation

Fig. 3.12 shows a schematic diagram of a Current Transformer (CT). A CT consists of two windings around an iron core. The primary winding is essentially a current carrying conductor where current is to be sensed. CTs' work on the principle which is same to the principle of electromagnetic induction of power transformer. However, there are subtle

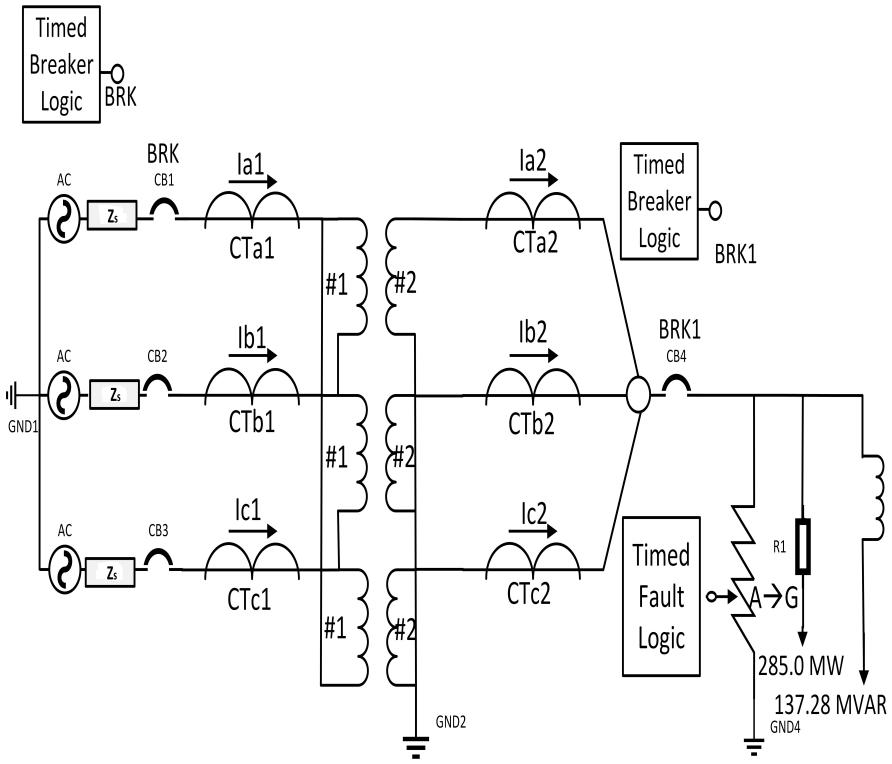

Figure 3.9: Circuit for external fault with CT saturation (source impedance $Zs = 0.0318\angle -88.1759$)

differences in their working which make them quite different from power transformers. The primary winding of the CT is connected in series with the load circuit in which the current is to be measured. There is no appreciable voltage between the two terminals of primary winding, and also this is very important that the primary current is obviously not determined by the secondary load or burden on the transformer. A replica of the primary current is expected to flow in the secondary circuit of the CT. The primary current as mentioned earlier does not depend on the burden connected on the secondary side. During normal operations, the flux in CT core is negligible as the flux produced due to secondary and the primary currents cancel each other. Thus in normal operations, the CTs provide quite accurate shape of the primary current on the secondary side as the core gives almost linear transformation for small flux density in the core. However, when transient condition occur there is change in the primary and secondary currents and the flux in the CT core becomes larger. If this difference in fluxes is quite large then the core enters into the saturation region. The saturation curve or the B-H curve is shown in Fig. 3.13. CT saturation is a complex phenomenon and modeling them accurately has been an active area of research. In the present thesis, CT saturation mathematical model used

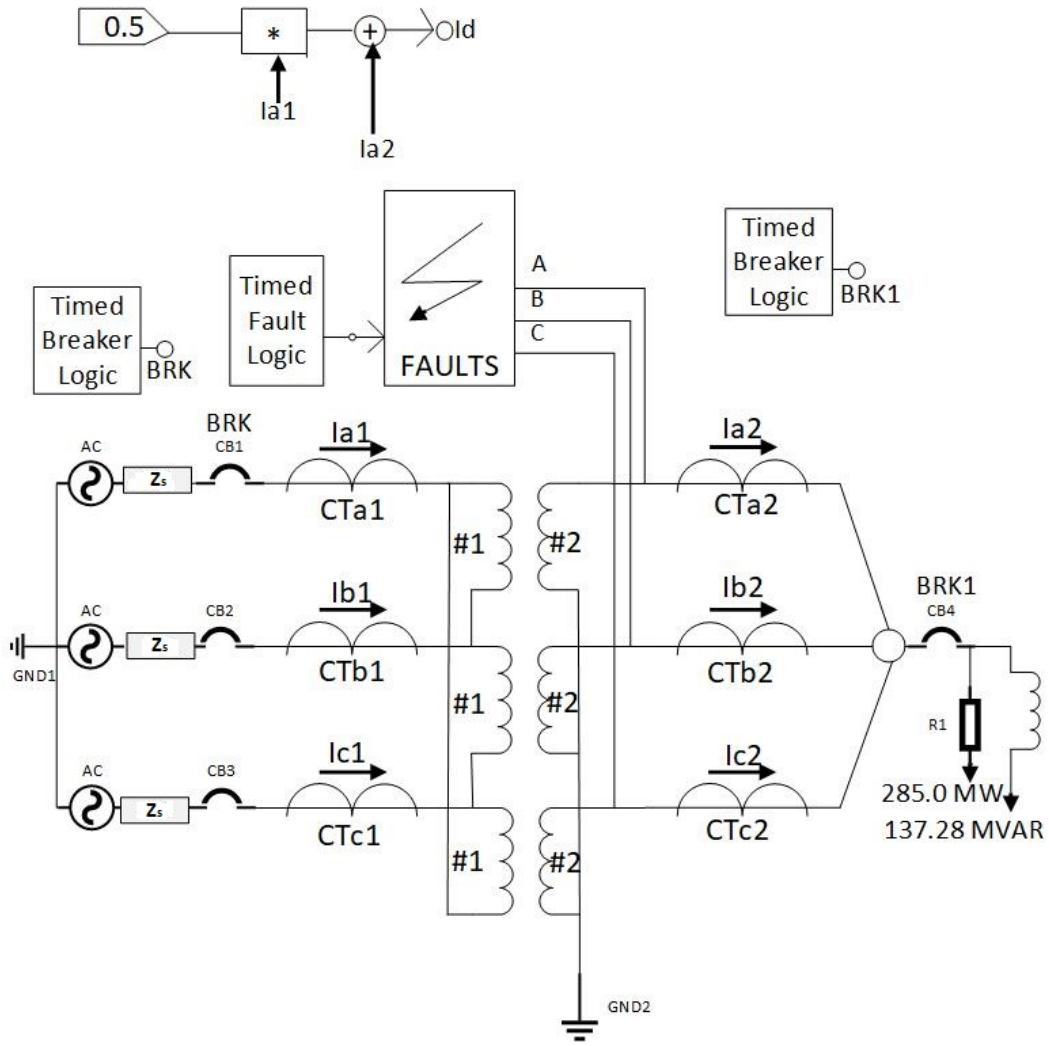

Figure 3.10: Test system for inrush and internal faults (source impedance $Zs = 0.0318\angle -88.1759$)

is Jiles and Atherton model [84] implemented in PSCAD.

The CT saturation may manifest itself in two forms namely, (i) Symmetrical saturation, and (ii) Asymmetrical saturation [85].

Symmetrical Saturation

In case of symmetrical saturation, the current in the primary winding of the CT tries to align magnetic dipoles present in the core. When the primary current is flowing with positive polarity, some of the magnetic dipoles are forced to align in one direction. The alignment of the magnetic dipoles in the core in with respect to the primary current at different instants (indicated as a, b, c, d, and e) are illustrated in Fig. 3.14. Initially, at

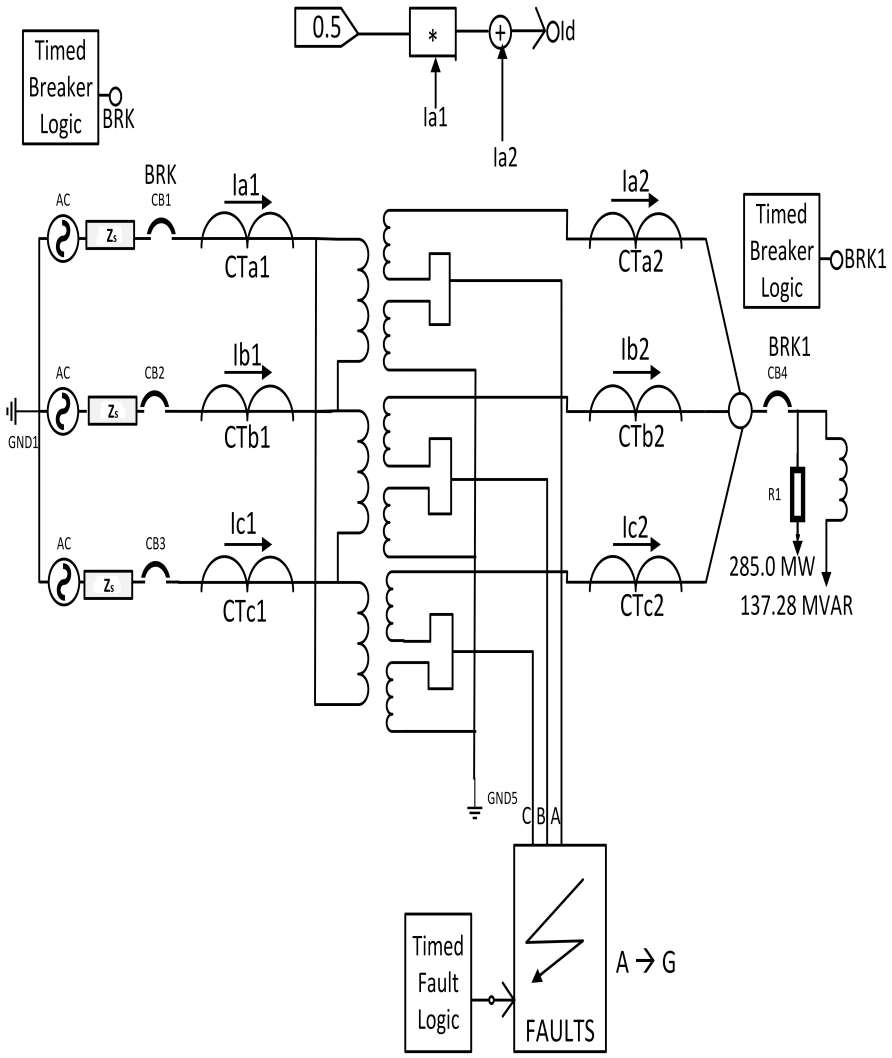

Figure 3.11: Circuit for internal fault with CT saturation at 60% winding (source impedance $Zs = 0.0318\angle - 88.1759$)

the instant a, all the magnetic dipoles are randomly aligned. From the instant a to b, as primary current gradually increase, aligned magnetic dipoles also increase in number. It is observed from the figure that at instant b, all the magnetic dipoles are aligned in one direction. Since all the magnetic dipoles are aligned, no change in flux occurs. This implies $\frac{d\phi}{dt}$ is zero, and hence V_s i.e. induced voltage in the secondary side of transformer becomes zero. This, in turn, results into zero secondary current. Fig. 3.14 (i) shows that the value of I_s falls to zero at position b. When the primary current I_p enters into its negative side at the instant c, then the secondary current also starts to decrease sinusoidally from zero in its in negative side. Due to change in polarity of I_p, the dipoles starts changing their alignment in opposite direction. This change in alignment changes flux and this

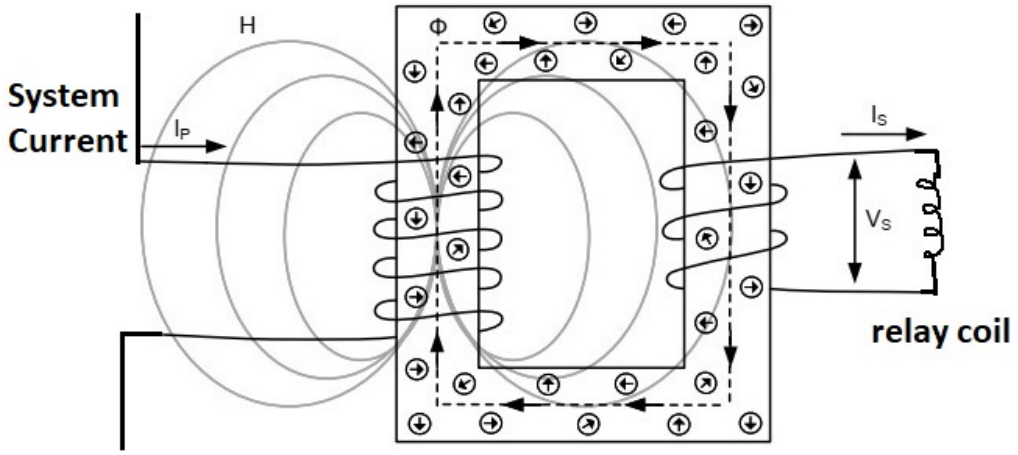

Figure 3.12: CT drawing

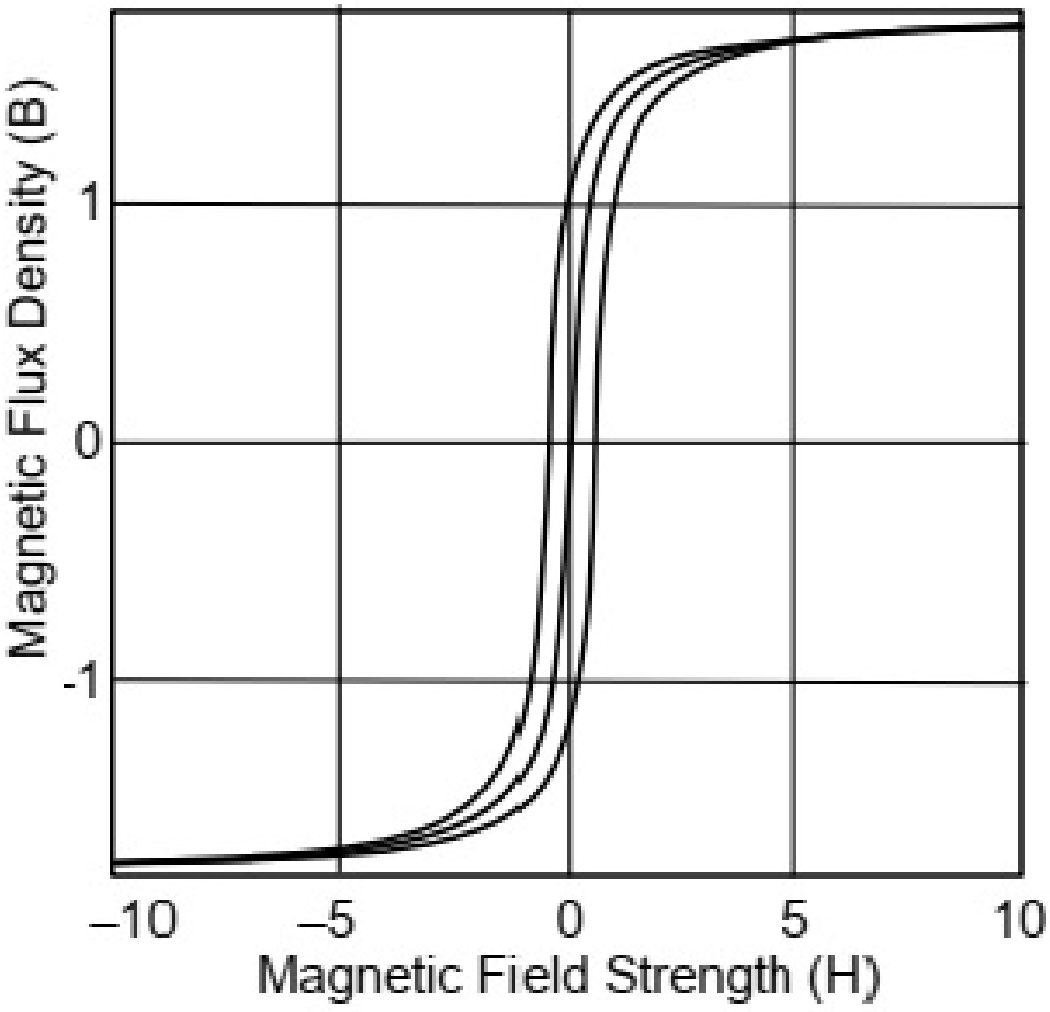

Figure 3.13: B-H curve example for different core materials

continues until all the dipoles are aligned and get saturated in opposite direction. At the instant d, when all dipoles are again aligned in same direction, the change in flux

becomes zero. Thus, I_s becomes zero at d. As the magnitude of the primary current reduces, the complete alignment of the dipoles does not happen and consequently $\frac{d\phi}{dt}$ does not become zero and the core comes out of the saturation. This phenomenon gives rise to symmetrical saturation in the positive and negative halves of the secondary current. This happens when primary current is high and symmetrical.

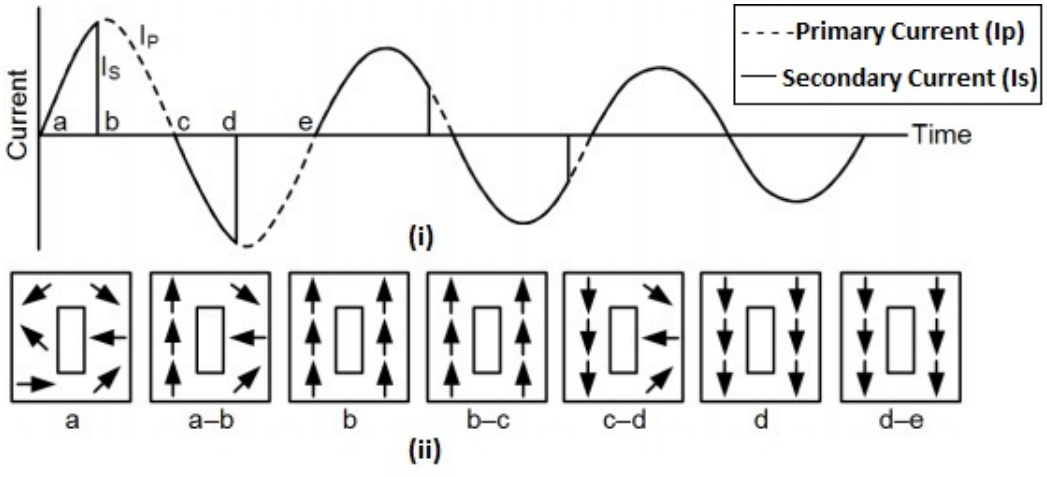

Figure 3.14: Primary currents, secondary currents, and magnetic dipoles in the core during symmetrical saturation

Asymmetrical Saturation

Due to presence of dc offset in the primary current, the primary current gets elevated on one of the sides. This implies that the primary current is not symmetrical about time axis as shown in Fig. 3.15 (i). Between points a and b, I_s and I_p follow the same trajectory. Due to flow of primary current I_p the magnetic dipoles in the core start to align in same direction. But, in this case all the dipoles do not get sufficient time to align in same direction in first half cycle. At position b, the secondary current changes to negative polarity, this causes some of the dipoles to move in opposite direction up to instant c. At point d, all dipoles get aligned in same direction. This completes the process of dipole alignment with flow of primary and secondary current as depicted in Figs. 3.15 (i) and (ii).

From the above description of symmetrical and asymmetrical saturation, it is observed that in symmetrical saturation the magnetic dipoles get aligned in first half cycle and so the saturation takes place in first half cycle of primary and secondary current. Whereas,

in asymmetrical saturation, state of maximum flux density is reached in more than one cycle of currents.

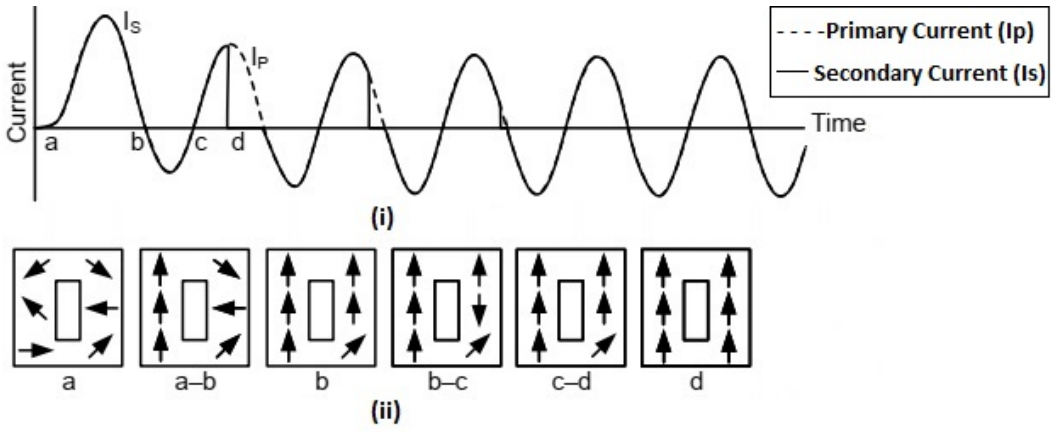

Figure 3.15: Primary currents, secondary currents, and magnetic dipoles in the core during asymmetrical saturation

3.2.4 Effects of CT Saturation on External and Internal Fault Signals

The performance of differential relay under CT saturation is one of the major issues that determines its robustness and efficacy. The CT saturation gives rise to prolonged restraint of the state-of-the-art relays during in-zone/internal faults [24]. Also there is a tendency of relays to operate during external faults due to presence of large dying out differential current.

The effects of CT saturation under *external* and *internal (inter-turn)* faults has been simulated using models given in Figs. 3.9 and 3.11 respectively. The CT parameters simulated in the model are given in Table. 3.1.

Effect of CT saturation on *External* fault Signals

Effects of CT saturation on external fault can be demonstrated using Fig. 3.16. The waveforms shown in Fig. 3.16 corresponds to the case where the fault takes place outside the protected zone (refer to Fig. 3.9). Since the fault is outside the protected zone, the primary current flows in both the CTs. The following observation pertaining to this case can be made.

Table 3.1: CT parameters for transformer

CT	**Primary side**	**Secondary side**
Primary turns	1	2
Secondary turns	160	160
Secondary Resistance	0.5ohm	0.5ohm
Secondary Inductance	0.8x10^{-3}H	0.8x10^{-3}H
Area	0.0001-0.0009m^2	0.0001-0.0009m^2
Path length	0.6377m	0.6577m
Remnant Flux Density	0.0T-0.5T	0.0T-0.5T
Burden Resistance	0.5ohm	0.5ohm
Burden Inductance	0.8x10^{-3}H	0.8x10^{-3}H

(i) Current waveforms in the primary and the secondary windings of the LT side CT are depicted Fig. 3.16(a) (in this response). It is observed that in this figure the saturation occurs only on one side of the CT secondary waveforms, i.e. on the negative side of the waveform. The positive side of the secondary waveforms is unison with the positive side of the primary current.

(ii) The HT side current waveforms in the primary and the secondary windings of the CT are depicted in Fig. 3.16(b). It is observed that in this figure the saturation occurs only on one side of the CT secondary waveforms, i.e. on the negative side only. The positive side of secondary waveform is in unison with the positive side of the primary current. It is also seen the saturation occurs on the secondary side of the CT.

(iii) The difference of the secondary side of the waveforms are plotted in Fig. 3.16(c). During external or through fault with heavy CT saturation, the amount of second harmonics in differential current is large. And also the time just after the saturation begins, is the time for the relay where it is very difficult to distinguish between in-zone and through faults. And since through fault is occurring outside protection zone, relay should not trip for this case. The CT must not saturate so heavily that trip occurs.

Effect of CT saturation on *In-zone* and *Internal* faults signals

This case shows the effect of deep CT saturation in presence of in-zone (within the protected zone) fault. Since the fault is inside the protected zone, current flows only in the source side CT. In the present work the fault at 60% of the winding's were considered for

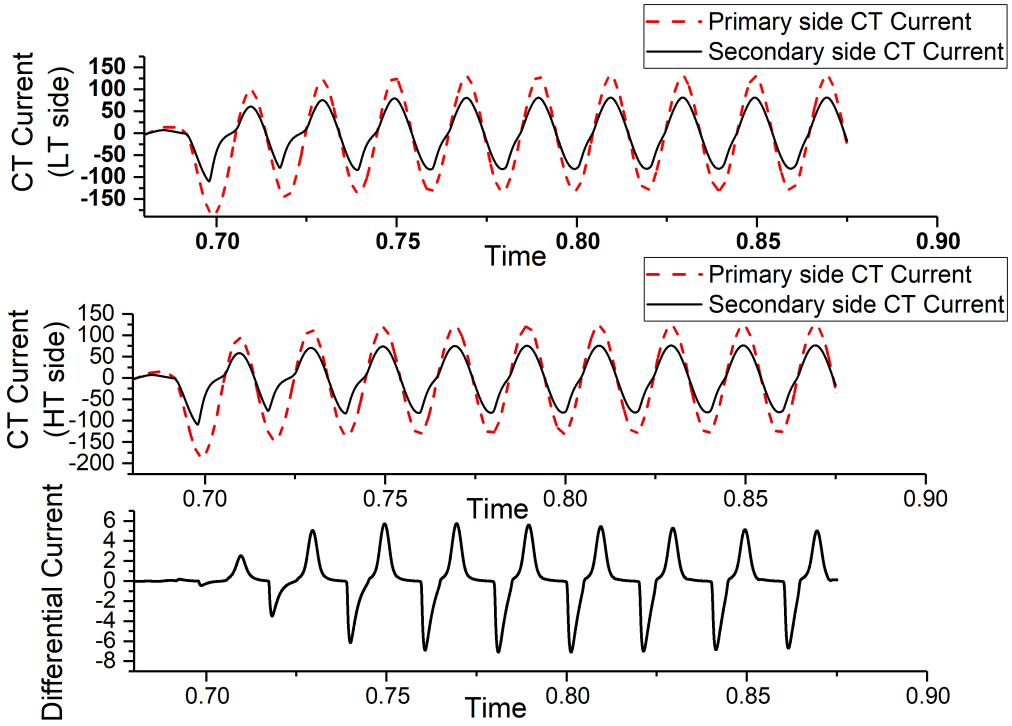

Figure 3.16: CT currents for external fault: (a) Primary and secondary CT (LT side) currents (b) Primary and secondary CT (HT side) currents (c) Differential current of the transformer

internal faults. To test the limit of performance of the proposed method, CT saturation levels were increased to the point, where the proposed method fails to detect the internal fault. This limiting case is also reported as poor CT case [24].

The differential current, which is essentially the CT's secondary current of the source side is depicted in Fig. 3.17(b). The figure also depicts the primary current of same CT. From the figure it is observed that,

(a) only the secondary side waveform of CT shows saturation effect. The primary waveform has no saturation.

(b) the secondary side waveform of CT shows the saturation effect on negative side of the sinusoid. The positive side remains same.

In case of in-zone and internal faults, secondary CT saturation current although contains fundamental component much larger than second harmonics, but due to heavy CT saturation, secondary side CT will output zero current for a large portion of a cycle. This may delay the trip decision. Hence, maximum time to come out of saturation should be calculated for worst case of in-zone and internal faults and it must be longer than the

time delay needed for tripping.

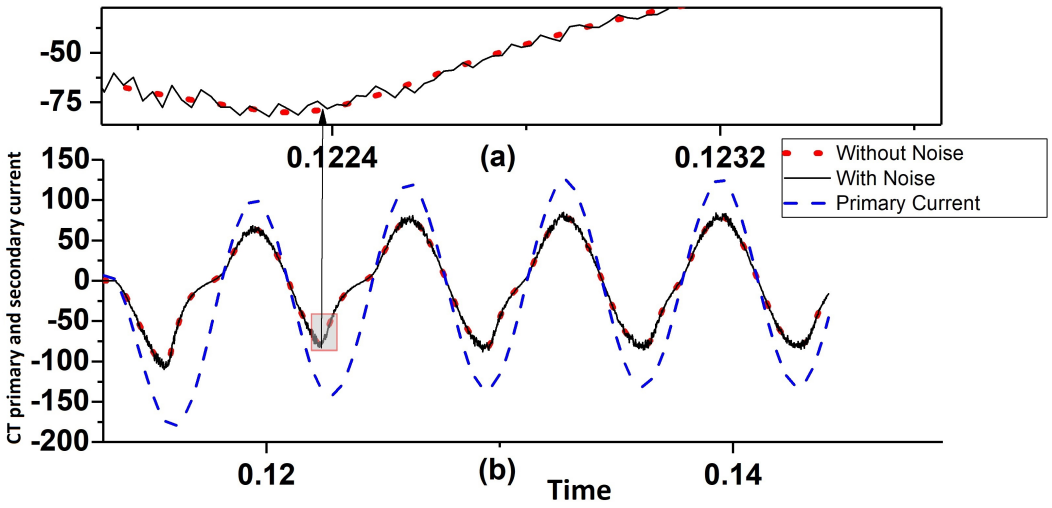

Figure 3.17: (a) Zoomed portion of CT secondary differential current (with and without noise) pertaining to in-zone fault (b) CT primary and CT secondary differential current (with and without noise) pertaining to in-zone fault

Fig. 3.18 shows the effect of deep CT saturation in presence of internal fault on 60 percent of the winding.

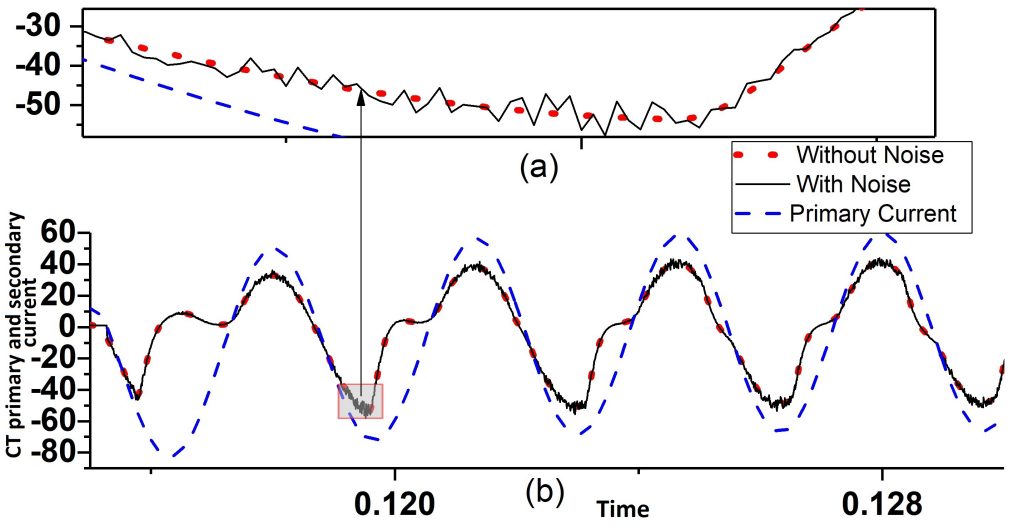

Figure 3.18: (a) Zoomed portion of CT secondary differential current (with and without noise) pertaining to internal fault (b) CT primary and CT secondary differential current (with and without noise) pertaining to in-zone fault at 60 % of transformer winding

3.2.5 Transformer Ratings

To study the robustness of the proposed method, the performance was also tested on the transformers of different ratings. Three transformers of rating 25 MVA, 315 MVA, and 200 MVA were taken for testing. The transformers are simulated on two different platforms namely MATLAB and PSCAD. It is to argue that the performance of proposed algorithm does not rest on the methods of simulations. For this reason the 25 MVA transformer was simulated in MATLAB (Fig. 3.19) whereas 315 and 200 MVA transformers were simulated in PSCAD. The simulation data used for 25 MVA transformer are given in Table 3.2. Table 3.3 shows the complete specification of 315 MVA and 200 MVA transformers used in PSCAD simulations.

Table 3.2: Transformer Model Parameters for MATLAB

Transformer	Transformer winding parameter	Transmission line parameters
25 MVA, 50 Hz	150 kV: R_1=0.02 pu, L_1= 0.08 pu 75 kV: R_2 = 0.02 pu, L_2 = 0.08 pu Configuration: Y-Y	r_0 = 0.3864 Ohms/km, r_1=0.01273 Ohms/km l_0 = 4.1264 mH/km, l_1 = 0.9337 mH/km c_0 = 7.751 nF/km, c_1 = 12.74 nF/km length=10 km

Table 3.3: Transformer Model Parameters for PSCAD Simulator

Transformer	315 MVA, 50 Hz	200 MVA, 50 Hz
Transformer winding parameter	400/200 kV	220/110 kV
Air core reactance	25.356 Ω	12.1 Ω
Magnetizing current	45.46 A	52.4875 A
Knee Voltage	1.17 pu	1.17 pu
Leakage reactance	0.1 pu	0.1 pu

3.2.6 Robustness

To test the robustness of the proposed method, uniformly distributed noise of ±5% was added to the waveforms. The tests were conducted for signals without noise and with noise and the results were compared to ascertain the robustness of the proposed method.

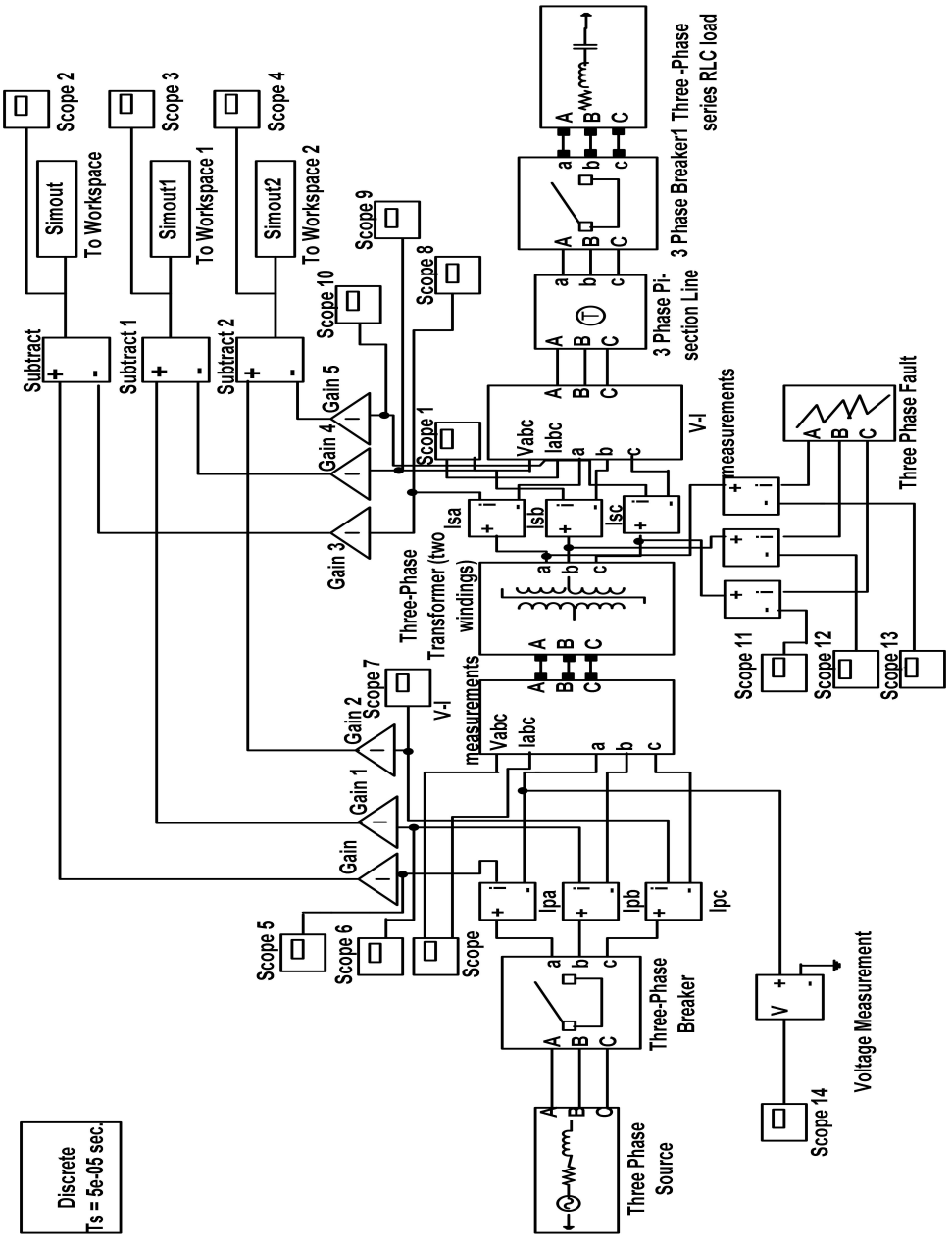

Figure 3.19: Simulink test system

3.3 Transformer Differential Protection Scheme

In this section, existing transformer differential protection scheme has been discussed as a background for the proposed scheme of transformer differential protection.

3.3.1 Existing Transformer Differential Protection Scheme

Conventional logic set-up for restraining the relay operation may be shown as an schematic of Fig. 3.20. The scheme is fundamental even to date. Fig. 3.20 shows that relay is activated when a current beyond a certain threshold is detected. An inrush (-restraining) processing unit processes the waveform and accordingly outputs either 1 (for no-inrush waveform) or 0 (for inrush waveform). The timing module coordinates the inrush processing unit and the gating logic to adjust for computation and processing delays depending on the method used. From the scheme of Fig. 3.20, it is evident that the detection time is essentially decided by inrush processing unit and that is the amount of time for which the fault current has to flow through the transformer before trip signal is issued in case of a in-zone fault. It is well known that there are several cases where the fault waveforms have resemblance to inrush waveforms. This resemblance is measured in terms of second harmonic component in relay schemes. Depending on the amount of second harmonic present, the restrain is applied on the trip signal. This method of applying restrain, delays the trip signal till the in-zone fault waveform have sufficiently reduced resemblance (second harmonics) to inrush waveforms. Thus, the fault current flows through the transformer up to the time for which no inrush is detected.

3.3.2 Proposed Scheme for Transformer Differential Protection

The current work has following two novel contributions; (i) a scheme for differential protection of transformer using independent detection of the fault and the inrush, and (ii) development of optimal matched wavelets enabling to use the scheme proposed in (i).

Fig. 3.21 shows a schematic logic set-up of a novel scheme proposed in this work, on the basis of *independent* detection of fault and inrush waveforms. In this scheme, the fault and the inrush are detected separately and simultaneously, however, there are times when the fault is detected first and there are situations where the inrush may be detected early. It is observed that unlike the conventional scheme, the trip decision is taken not on

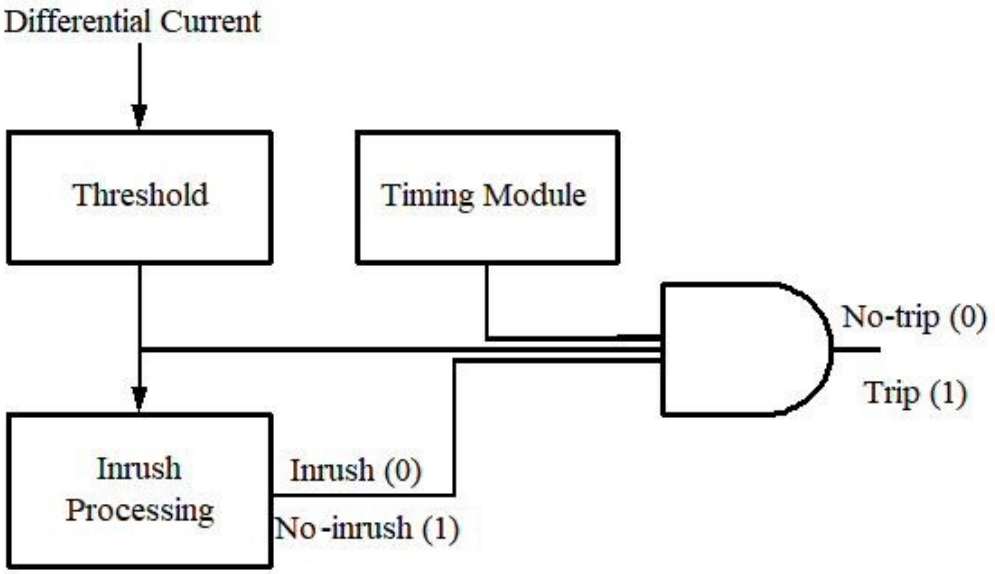

Figure 3.20: A schematic logic set-up for relay operation (Existing Scheme)

the basis of inrush detection rather trip decision is taken on the basis of fault detection. It is observed that the time elapsed for which the fault current has to flow through the transformer is one which is lowest among the detection times of inrush processing unit and fault processing unit. The scheme is also capable of handling the case when fault current has high resemblance to inrush current (such as external fault and in-zone faults under high level of CT saturation). The scheme can output the presence of inrush-resemblance and presence of fault-resemblance, simultaneously, and decision is made accordingly. This avoids applying unnecessary restraints in situations of in-zone/internal faults under CT saturation. The outputs of both the processing units give the full information regarding trip signals for post-event analysis.

It is due to the simultaneous detection capability of *Inrush Processing* unit and *Fault Processing* unit that the scheme proposed in Fig. 3.21 can be conceived and implemented for differential protection. In the present work optimal matched wavelets are developed for *Inrush Processing* and *Fault Processing*. The efficacy of the developed inrush wavelet is validated with the existing wavelets used in literatures [53] [54] [82] [80] [81] (refer to section 2.6.1 of chapter 2). The development of matched wavelet for detecting fault waveform independent of inrush is reported for the first time through this work. The matched wavelets are developed to work on first level of coefficients which reduces the computations drastically, whereas, most of the methods use higher level coefficients for

detection resulting in large computations. Further, going for higher levels of coefficients makes the methods prone to noise which is inherent in such signals. The method developed is also tested to work under ±5% of uniformly distributed noise.

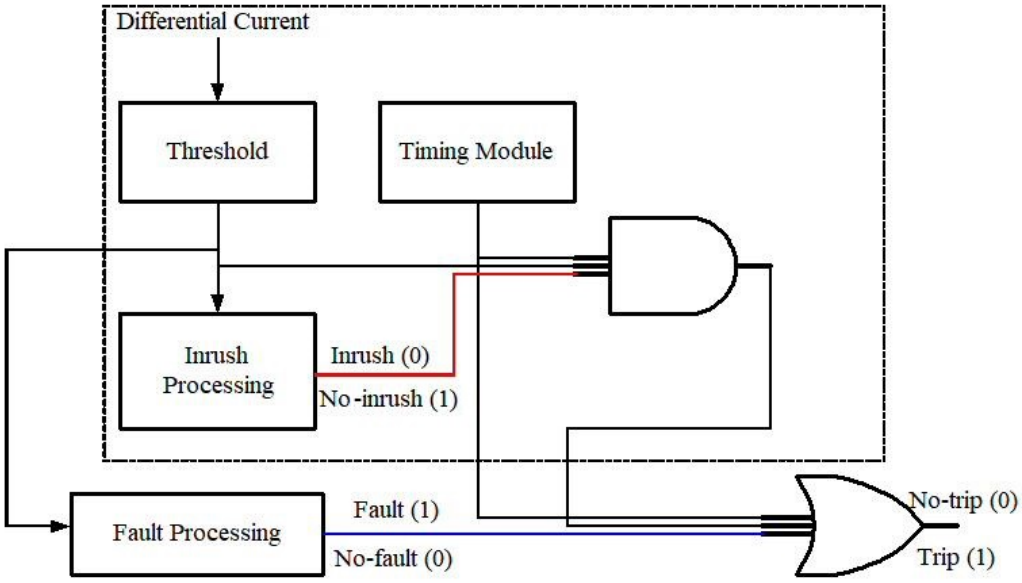

Figure 3.21: A schematic logic set-up for relay operation (Proposed Scheme)

3.3.3 Matched Wavelets for Inrush and Fault Waveforms

The matched wavelets were determined for differential inrush and fault waveforms separately as discussed in section 2.6 of Chapter 2. For the purpose of designing the fault wavelet, an L-G fault was taken. The waveform used was of the phase which was faulted. The differential inrush and the fault waveforms obtained from 25 MVA transformer were used to design a mother wavelet. Typical characteristic shapes of inrush and fault waveforms at 0° are shown in Fig. 3.22 and Fig. 3.23 respectively. Designing a matched mother wavelet from a waveform is equivalent to obtaining a basis function which captures some characteristic features of the waveform. Depending on the number of coefficients, N, and number of constraints, several basis functions can be generated. Few of the possible basis functions obtained are depicted in Fig. 3.22 and Fig. 3.23 for inrush and fault waveforms respectively. All these wavelets capture some characteristic features of the waveforms of interest. The best basis function or the matched wavelet is decided on the basis of performance obtained when tested for detection efficiency. If an appropriate characteristic is captured by the mother wavelet, then a single wavelet can be used for different switching

angles and different inrush conditions such as, over fluxing and sympathetic inrush. If there are several available mother wavelets capturing the appropriate characteristics, the one with lower number of filter coefficients is preferable for hardware implementation.

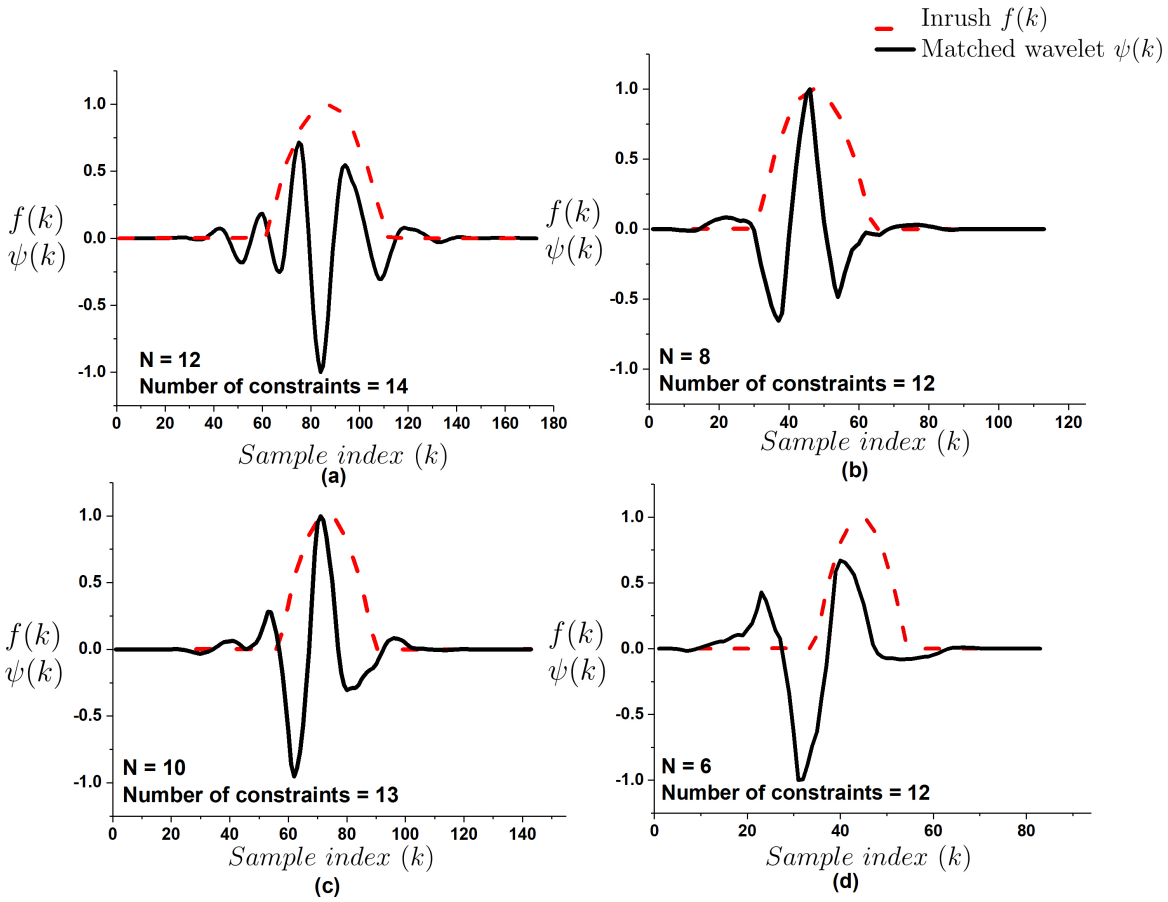

Figure 3.22: Inrush waveform and matched inrush wavelets

Threshold Determination

The representative inrush and fault waveforms are shown in Fig. 3.24(a). Example responses are shown in Fig. 3.24(b) and Fig. 3.24(c) for inrush-filter and fault-filter respectively. It can be observed that in case of inrush-filter (Fig. 3.24(b)) the inrush part of the waveform shows high values of coefficients (response) whereas, the fault part of waveform shows very small values of the coefficients (response). In the case of fault-filter response (Fig. 3.24(c)), fault part of waveform shows high values of coefficients (response) and lower values for inrush part of waveform. For the inrush-filter, the maximum value of response for fault waveform determines the threshold value at that switching angle (refer

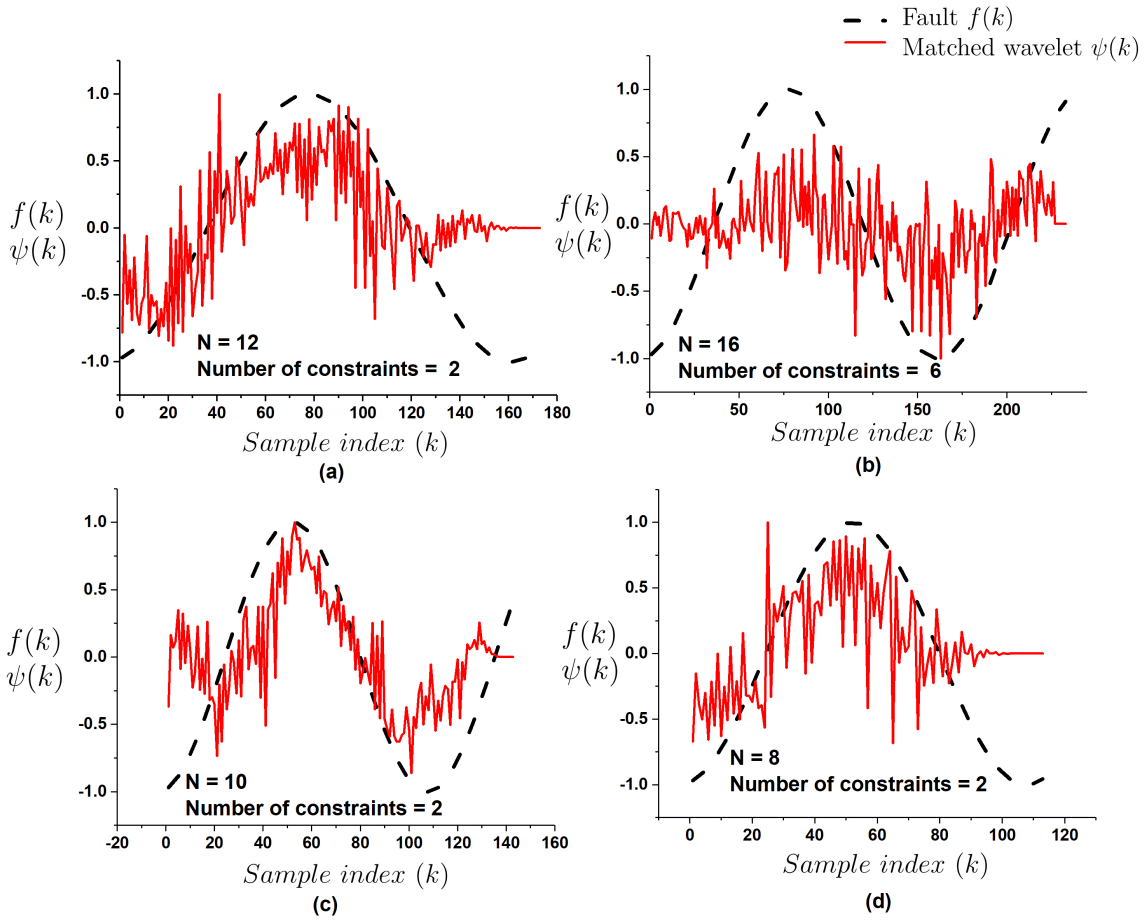

Figure 3.23: Fault waveform (L-G fault) and matched fault wavelets

Fig. 3.24(b)). Following procedure was used to determine the threshold for the fault filter.

1. The inrush waveforms at all the switching angles (in the interval of 5 degrees) are generated. The response of fault-filter to all of these inrush cases were obtained. The maximum value of the fault-filter response among all the inrush waveforms was taken as threshold for the fault-filter. Thus, the threshold selected was determined for the worst case scenario out of all the switching angles of inrush currents. In fact, practically, we have covered all possible cases for determining the threshold.

2. The fault-filter takes the normalized waveforms as input, thus there is no bias for the actual magnitude of the waveforms. All waveforms are scaled to have a peak/valley of 1/-1.

3. From the above two cases, it is highly unlikely that the inrush may be mis-detected as fault. As far as present studies are concerned, no such case was found. A similar

procedure was applied for determining the threshold for the inrush filter.

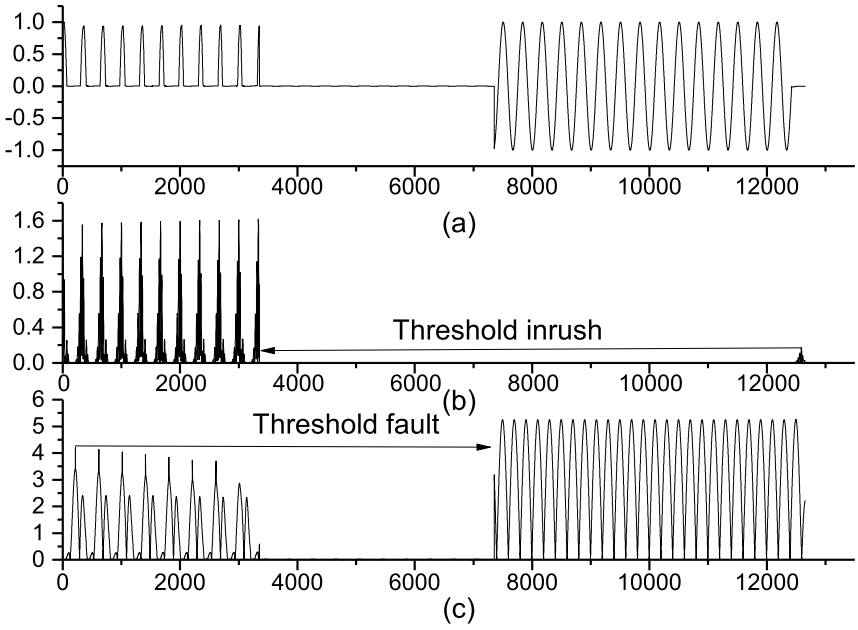

Figure 3.24: (a) Normalized differential current waveform (b) Response of inrush-filter (c) Response of fault-filter

Table 3.4 shows the threshold values obtained for various switching angles and the associated number of cycles elapsed before the inrush-filter reaches the threshold value. From the table, it is observed that the final threshold value obtained is 0.08 for the 25 MVA transformer and the worst case scenario takes 0.228 cycles for detection i.e. maximum time taken for detection of inrush.

3.4 Results and Discussion

For the purpose of testing the performance of the proposed method, the inrush and fault waveforms were generated for different switching angles. The range of test conditions and associated circuits are already described in section 3.2. Fig. 3.25(b) shows magnetizing inrush current and its noisy ($\pm 5\%$) version in Fig. 3.25(a) for 315 MVA transformer. The response of inrush-filter for the magnetizing inrush current and its noisy counterpart is depicted in Fig. 3.25(c). It can be observed that the response of inrush-filter consistently

Table 3.4: Threshold and Worst Case Detection Scenario for Inrush Wavelet Filter (K=12, Number of Constraints=14)

Switching angles	**Threshold value**	**Detection cycles**
0-15	**0.08**	0.174
20-30	0.08	0.178
35-40	0.08	0.174
45-50	0.08	0.1771
55	0.08	0.2102
60-120	No Inrush	No inrush
125-140	0.08	0.174
135	0.08	0.1874
140	0.08	0.21
145	0.08	**0.228**
150-155	0.08	0.191
160-180	0.08	0.174

crosses the inrush threshold. The speed of response is almost instantaneous. The response of fault-filter for the magnetizing inrush current and its noisy counterpart is depicted in Fig. 3.25(d). It can be observed that the response of fault-filter for inrush waveform remains below the fault threshold. A similar set of figures depicting the case of over-excitation and sympathetic inrush (under no-load) are given in Fig. 3.26 and Fig. 3.27 respectively. Fig. 3.28 shows the response of inrush-filter and fault-filter for sympathetic inrush under loaded condition. From the inrush-filter response shown in Fig. 3.28(b), it is observed that the response of inrush-filter is not crossing the threshold. Also, it is observed that the response of fault-filter (Fig. 3.28(c)) does not cross the threshold. It may be observed that the waveform do not have any appreciable resemblance to an inrush waveform. However, it is seen that the fault-filter correctly detects the presence of no-fault. Similarly, Fig. 3.29 shows the response of inrush- and fault-filter for inrush current 25 MVA transformer simulated in MATLAB environment. The testing was performed for 50 magnetizing inrush cases, 30 over-excitation cases, and 20 sympathetic inrush cases for the said three transformers. The results in terms of fraction of cycles the proposed method takes to detect the inrush are summarized in Table. 3.5.

The analysis of the fault waveforms and its noisy counterparts, using inrush-filter and fault-filter, were also performed. Fig. 3.30(b) shows the differential waveform for an LG fault on 315 MVA transformer. The noisy counterpart of the fault waveform is also

depicted on the same figure. The response of the inrush-filter for the waveform is shown in Fig. 3.30(c). It is observed that the response of inrush-filter is consistently below the inrush threshold. Fig. 3.30(d) which shows the response of the fault-filter, clearly detects the fault situation consistently for noisy as well as actual waveform. Similarly, Fig. 3.31 shows the responses of the inrush- and fault-filters for in-zone fault for 25 MVA transformer. Analysis of a case of energisation under in-zone fault (L-G fault) is shown in Fig. 3.32. It is observed from Fig. 3.32(c) that the response of inrush-filter clearly detects that there is no-inrush present in the waveform of Fig. 3.32(b), whereas, Fig. 3.32(d) shows that the response of fault-filter clearly depicts the presence of fault phenomena. Thus, in case the transformer is energized in presence of fault, the fault can be successfully detected with the proposed fault-filter, whereas in conventional relay the inrush restraint method would allow the fault current to flow through the transformer. Further, the detection efficacy of the proposed method was studied for the case of in-zone fault with three representative values of fault resistances viz. 0.1 (pu), 0.5 (pu), and 1 (pu) and the corresponding responses (inrush-filter and fault-filter) are shown in Figs. 3.33, 3.34, and 3.35 respectively. From the figure it is observed that the proposed method correctly detects the in-zone faults with fault resistances than that of the conventional scheme as mention in Chapter 3 section 3.3.1. The performance of the transformer under high degree of CT saturation was studied for external faults, and one of the detection scenario is depicted in Fig. 3.36. Fig. 3.36(a) depicts the noisy counterpart of simulated waveform for external fault (L-G fault) in presence of CT saturation. Fig. 3.36(b) depicts the external fault current under CT saturation. The response of the inrush-filter, shown in Fig. 3.36(c), detects inrush phenomena in the waveform. It is observed that, the external fault signal resulting due to CT saturation resembles quite similar to an inrush waveform except for the fact that it is bi-directional in nature. The response of the fault-filter, shown in Fig. 3.36(d), detects that there is no in-zone fault or internal fault in the transformer, thereby signaling no-trip signal (refer to section 3.3.2 for proposed relaying scheme), which saves the relay from mal-operation. It is observed that the relay clearly signals no-fault along with high resemblance of waveform with inrush waveform. A similar worst case scenario, for the detection of in-zone fault in presence of severe CT saturation is depicted in Fig. 3.37. The worst case scenario here pertains to the fact that, although, the trip decision was correctly made (detected correctly as fault), the

inrush-filter failed to detect no-inrush condition in such cases. A similar case is depicted for internal fault (inter-turn) with fault involving 60 percent of the winding in Fig. 3.38. In this case also, a correct detection is made. From the figure, it can be seen that the relay clearly indicates an internal fault bearing very high resemblance to inrush waveform, however, the trip signal is generated in this case without any restraint (refer the proposed differential scheme given in section 3.3.2). Thus, it is observed that the saturation part of the waveform resembles inrush current as detected by the inrush-filter however, the waveform is essentially a fault waveform which is correctly detected by the fault-filter. Thus, the scheme handles the case when the fault currents have high resemblance to the inrush currents. Other cases of inter-turn faults are depicted in Figs. 3.39, 3.40, 3.41, and 3.42 for fault involving 20%, 10%, 5%, and 2% of the windings respectively. It is observed that the proposed fault-filter correctly detects the presence of fault involving 20%, 10%, and 5% of the windings and inrush-filter detects absence of inrush. The case where the inter-turn fault could not be detected was the case with 2% of the inter-turn winding involved in secondary side of transformer. However, the proposed method has ability to detect the inter-turn fault up-to 5% of the winding. The associated hysteresis loop for the CT is depicted in Fig. 3.43. A case where the detection fails due to poor CT is depicted in Fig. 3.44 [24].

Thus, it can be seen that the proposed methods is robust to noisy conditions and CT saturation effects. It is worth noting that methods those rely on the harmonic restraints depends on detecting $3-5\%$ of the higher harmonics. Such methods may mal-operate in noisy conditions.

The summary of results for detection of fault cases for different types of faults is depicted in Table 3.6. From Table 3.6 and 3.5 it observed that for 315 MVA transformer, the minimum fraction of cycle to detect a two phase fault is 0.1 cycle which is less than maximum fraction of cycle to detect a sympathetic inrush case i.e. 0.153 cycle. Thus, in practical scenarios there could be situations where fault could be detected faster than the inrush. This makes the scheme of Fig. 3.21, of detecting fault and inrush independently, advantageous over the traditional scheme of Fig. 3.20.

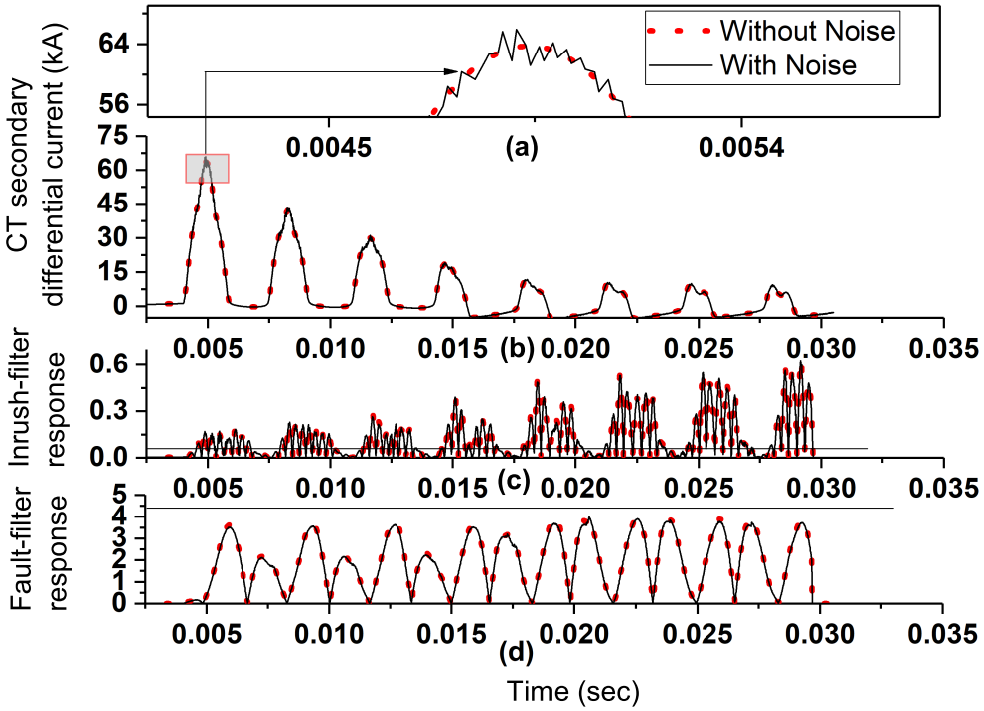

Figure 3.25: Case of magnetizing inrush and its noisy version for 315 MVA transformer, angle of inception 0° (a) Zoomed portion of CT secondary differential current (b) CT secondary differential current (c) Response of inrush-filter (d) Response of fault-filter

Table 3.5: Summary Results for Inrush Detection

	Magnetizing inrush(50 cases)		**Overfluxing (30 cases)**		**Sympathetic inrush(20 cases)**	
Detection cycles / Transformer ratings	min.	max.	min.	max.	min.	max.
315 MVA	0.001	0.012	0.01	0.08	0.099	0.153
200 MVA	0.003	0.018	0.009	0.096	0.1	0.42
25 MVA	0.174	0.228	0.177	0.312	0.415	0.51

Table 3.6: Summary Results for Fault Detection

	L-G fault (30 cases)		**L-L-L-G fault (30 cases)**		**L-L-L fault (30 cases)**		**L-L fault (30 cases)**	
Detection cycles / Transformer ratings	min.	max.	min.	max.	min.	max.	min.	max.
315 MVA	0.153	1.41	0.17	1.42	0.31	1.25	0.1	1.078
200 MVA	0.796	1.13	0.83	1.07	0.84	1.08	0.74	1.21
25 MVA	0.408	0.766	0.428	0.814	0.45	0.87	0.47	0.616

3.5 Summary

This chapter contributes a new differential protection scheme based on *independent* detection of fault and inrush waveforms. The development of matched wavelet for detecting

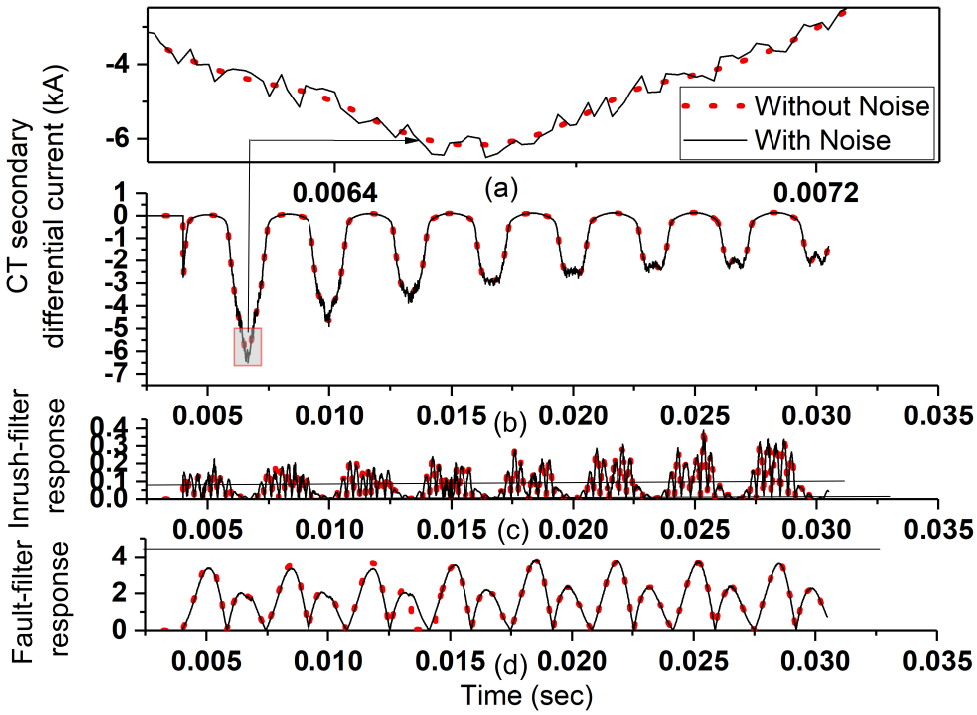

Figure 3.26: Case of over-excitation current and its noisy version for 315 MVA transformer, angle of inception 180° (a) Zoomed portion of CT secondary differential current (b) CT secondary differential current (c) Response of inrush-filter (d) Response of fault-filter

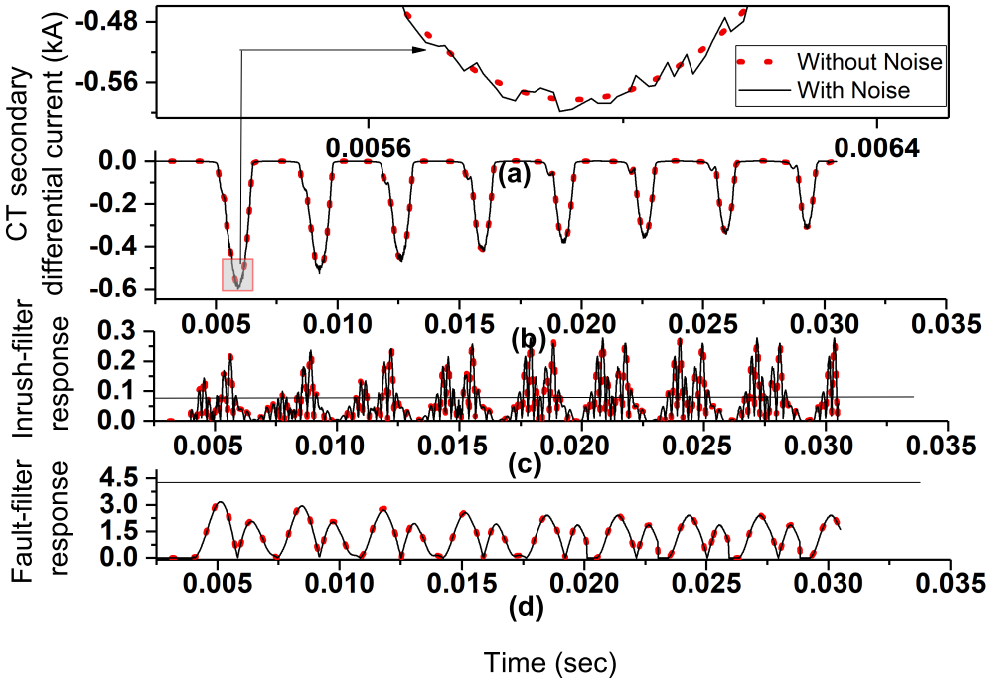

Figure 3.27: Case of sympathetic inrush current and its noisy version for 315 MVA transformer, angle of inception 180° (a) Zoomed portion of CT secondary differential current (b) CT secondary differential current (c) Response of inrush-filter (d) Response of fault-filter

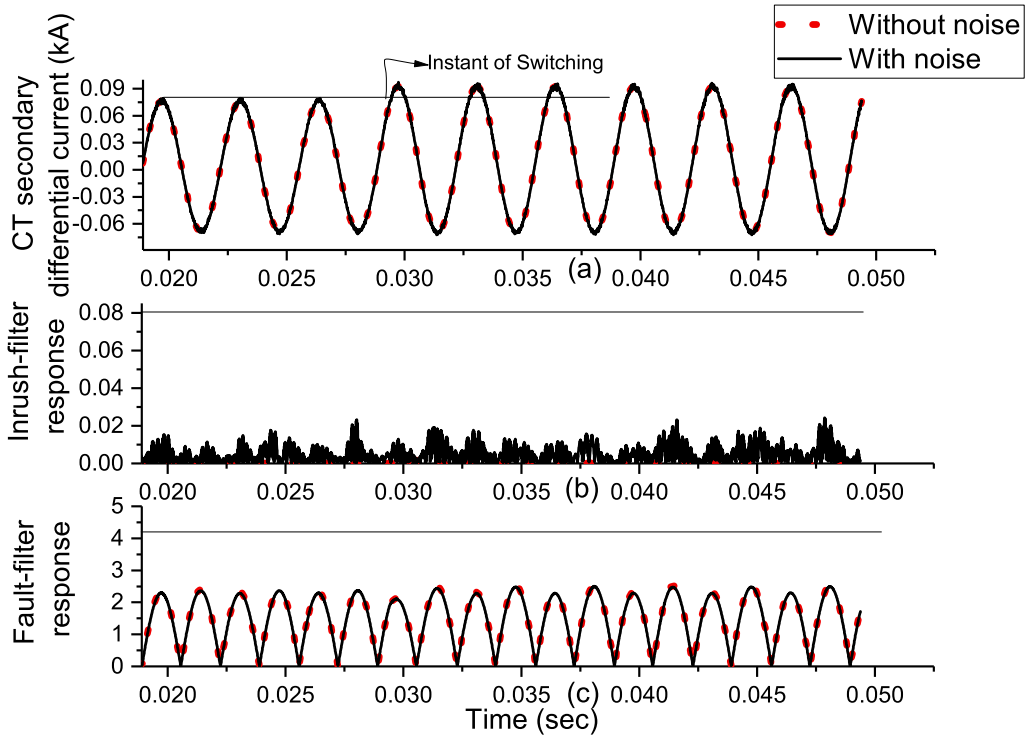

Figure 3.28: Case of sympathetic inrush current and its noisy version for 315 MVA transformer with load, angle of inception 0° (a) Zoomed portion of CT secondary differential current (b) CT secondary differential current (c) Response of inrush-filter (d) Response of fault-filter

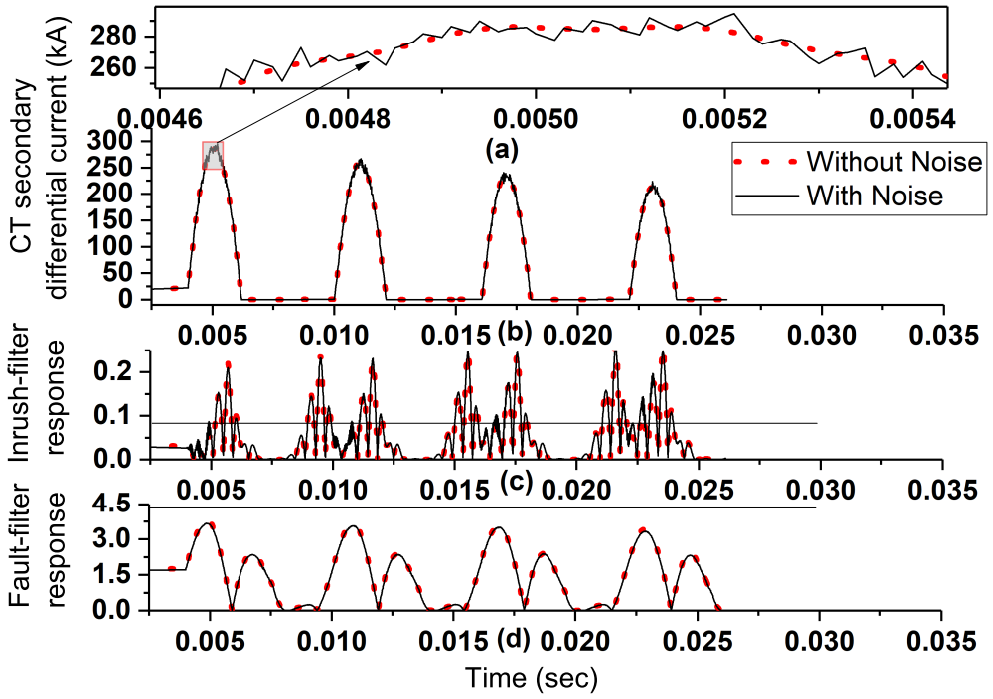

Figure 3.29: Case of magnetizing inrush current and its noisy version for 25 MVA transformer (a) Zoomed portion of CT secondary differential current (b) CT secondary differential current (c) Response of inrush-filter (d) Response of fault-filter

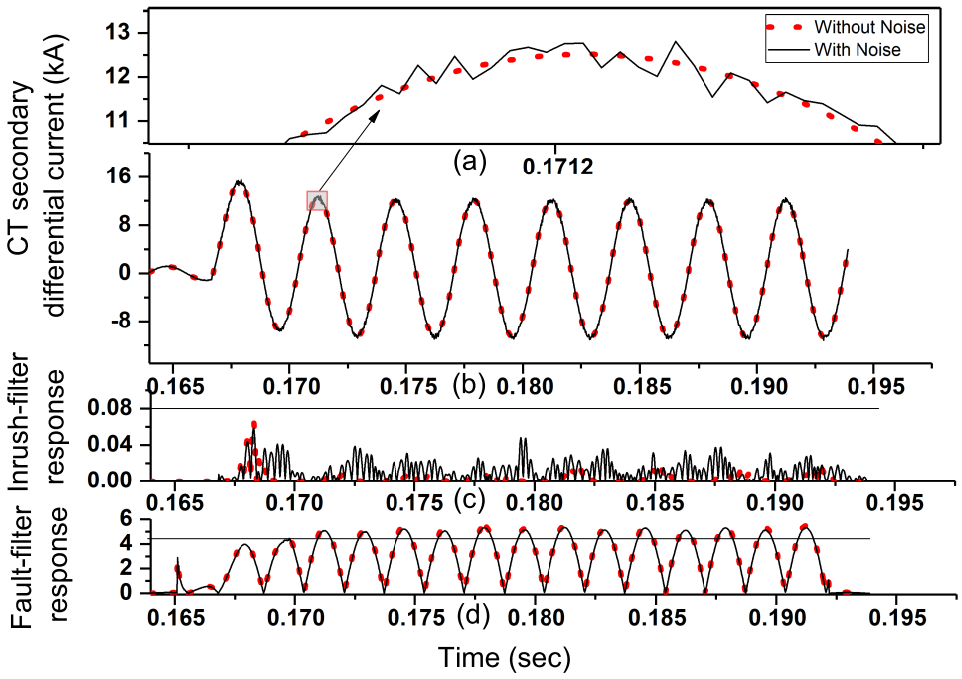

Figure 3.30: Case of L-G fault current and its noisy version for 315 MVA transformer, angle of inception 0° with fault resistance 0.01 *ohm* (a) Zoomed portion of CT secondary differential current (b) CT secondary differential current (c) Response of inrush-filter (d) Response of fault-filter

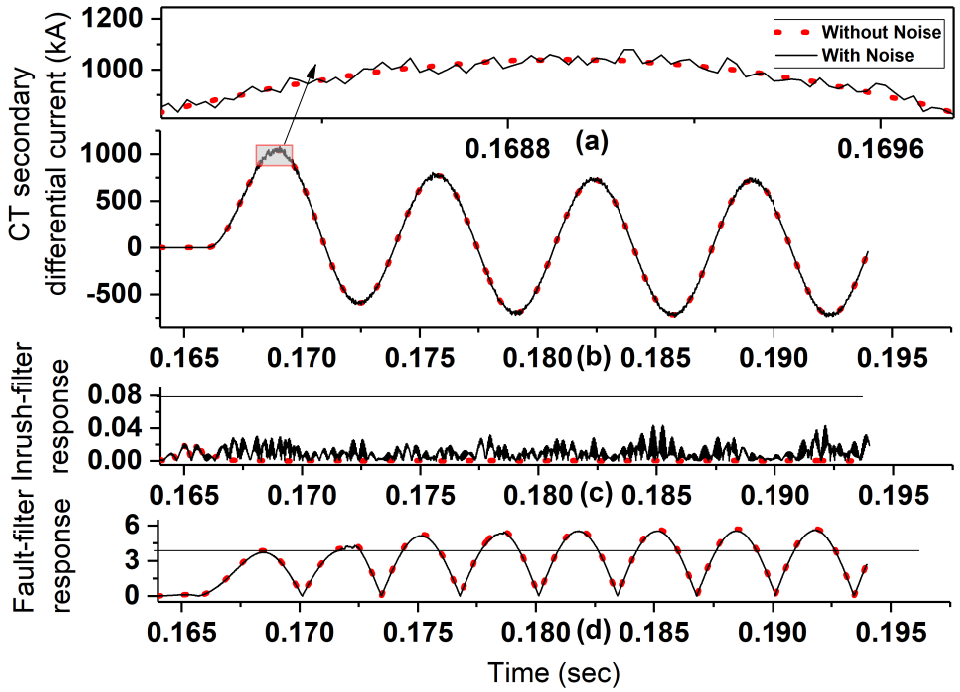

Figure 3.31: Case of L-G fault current and its noisy version for 25 MVA transformer, angle of inception 0° (a) Zoomed portion of CT secondary differential current (b) CT secondary differential current (c) Response of inrush-filter (d) Response of fault-filter

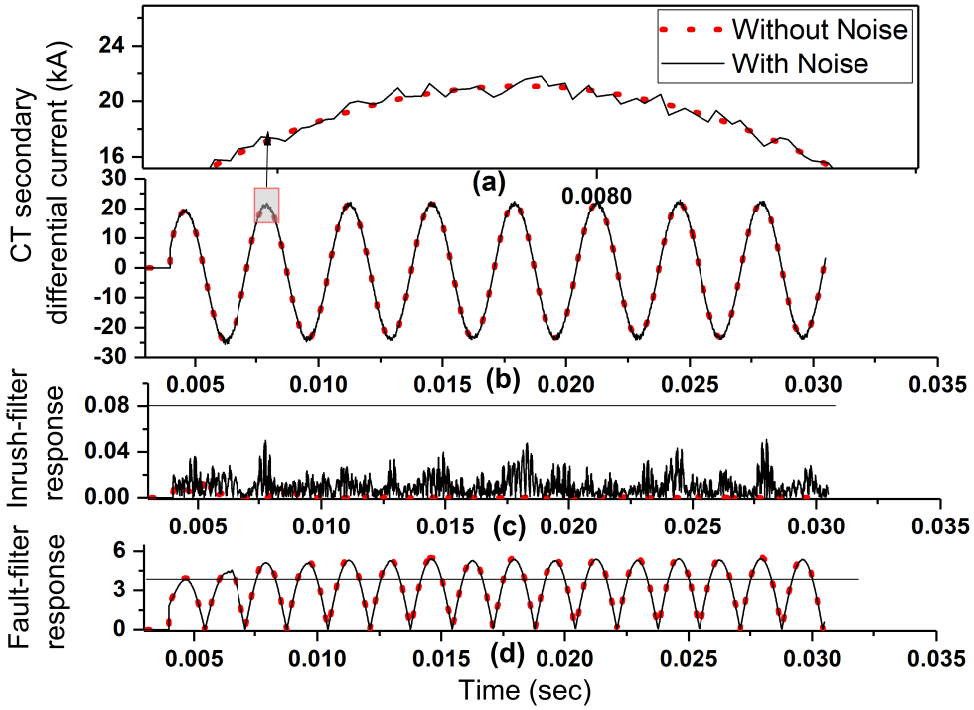

Figure 3.32: Case of 25 MVA transformer energized under fault (L-G fault) at 0° and its noisy version (a) Zoomed portion of CT secondary differential current (b) CT secondary differential current (c) Response of inrush-filter (d) Response of fault-filter

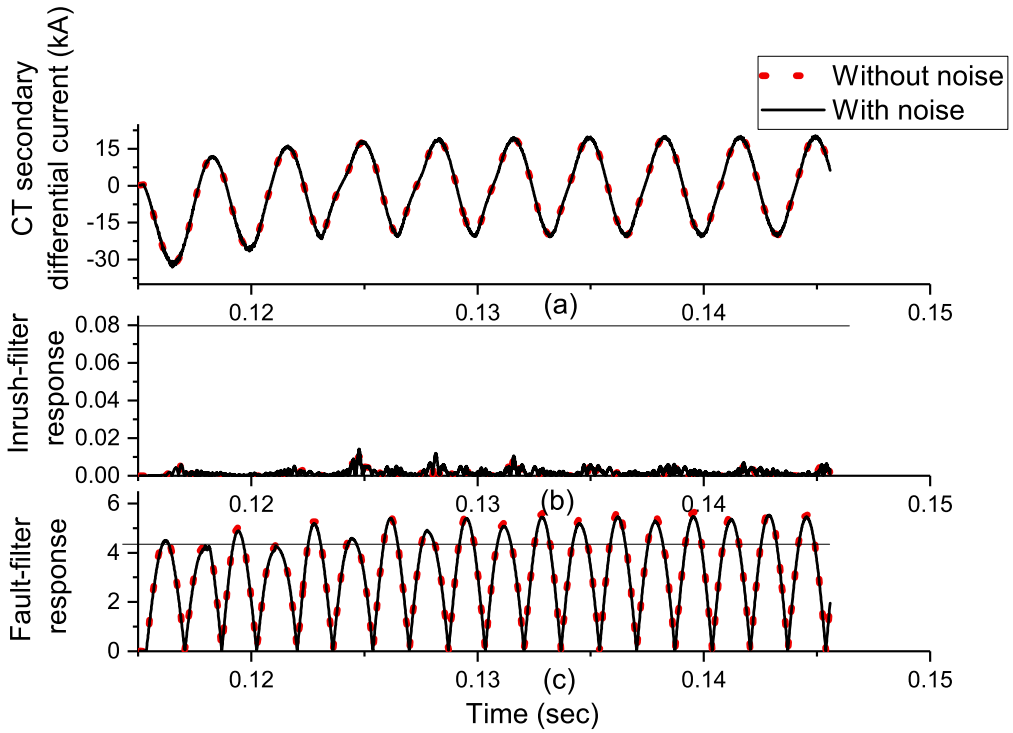

Figure 3.33: Case of L-G fault current and its noisy version for 315 MVA transformer with fault resistance 0.1 *ohm*, angle of inception 180° (a) Zoomed portion of CT secondary differential current (b) CT secondary differential current (c) Response of inrush-filter (d) Response of fault-filter

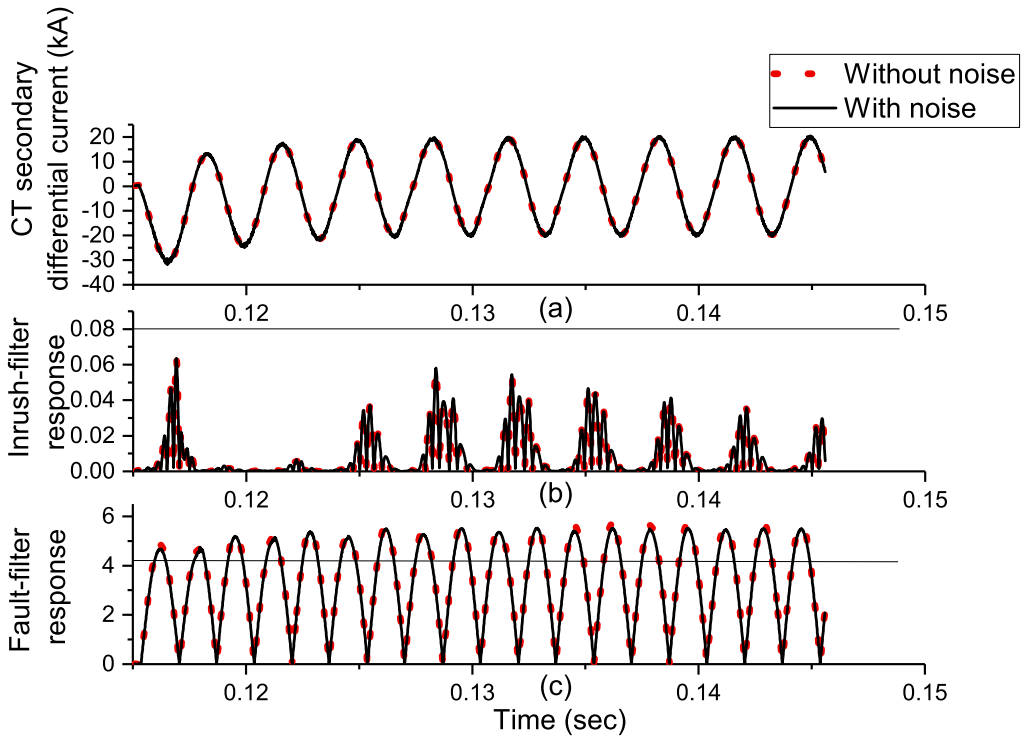

Figure 3.34: Case of L-G fault current and its noisy version for 315 MVA transformer with fault resistance 0.5 *ohm*, angle of inception 180° (a) Zoomed portion of CT secondary differential current (b) CT secondary differential current (c) Response of inrush-filter (d) Response of fault-filter

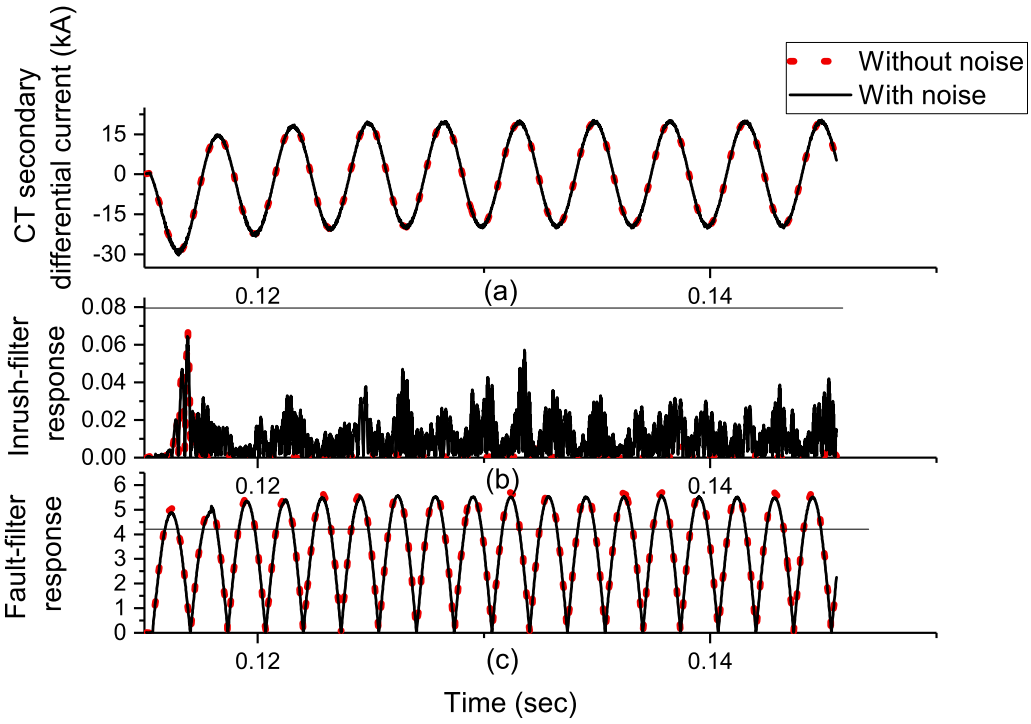

Figure 3.35: Case of L-G fault current and its noisy version for 315 MVA transformer with fault resistance 1 *ohm*, angle of inception 180° (a) Zoomed portion of CT secondary differential current (b) CT secondary differential current (c) Response of inrush-filter (d) Response of fault-filter

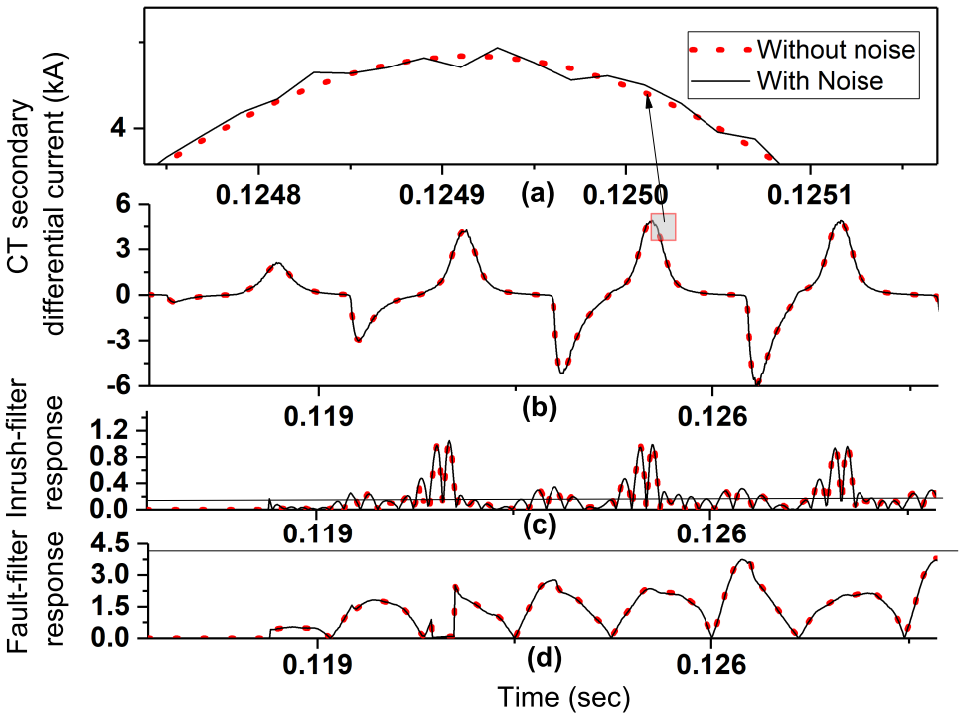

Figure 3.36: Case of external fault current and its noisy version for 315 MVA transformer, angle of inception 10° (a) Zoomed portion of CT secondary differential current (b) CT secondary differential current (c) Response of inrush-filter (d) Response of fault-filter

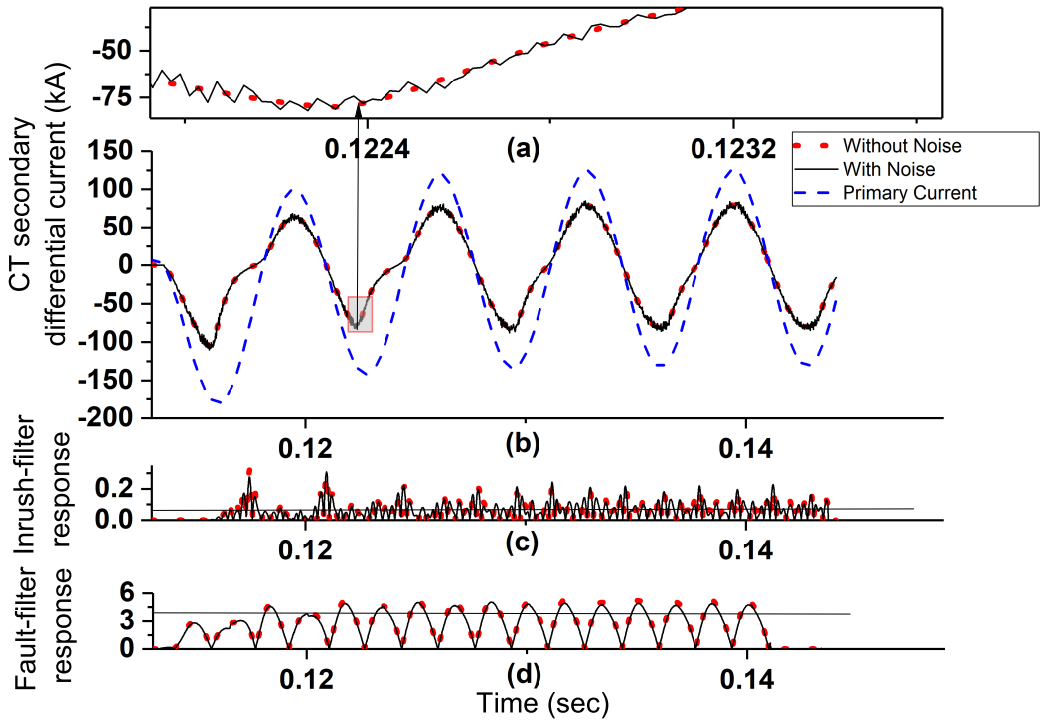

Figure 3.37: Case of L-G fault current and its noisy version under moderate saturation for 315 MVA transformer, angle of inception 0° (a) Zoomed portion of CT secondary differential current (b)CT primary and CT secondary differential current (c) Response of inrush-filter (d) Response of fault-filter

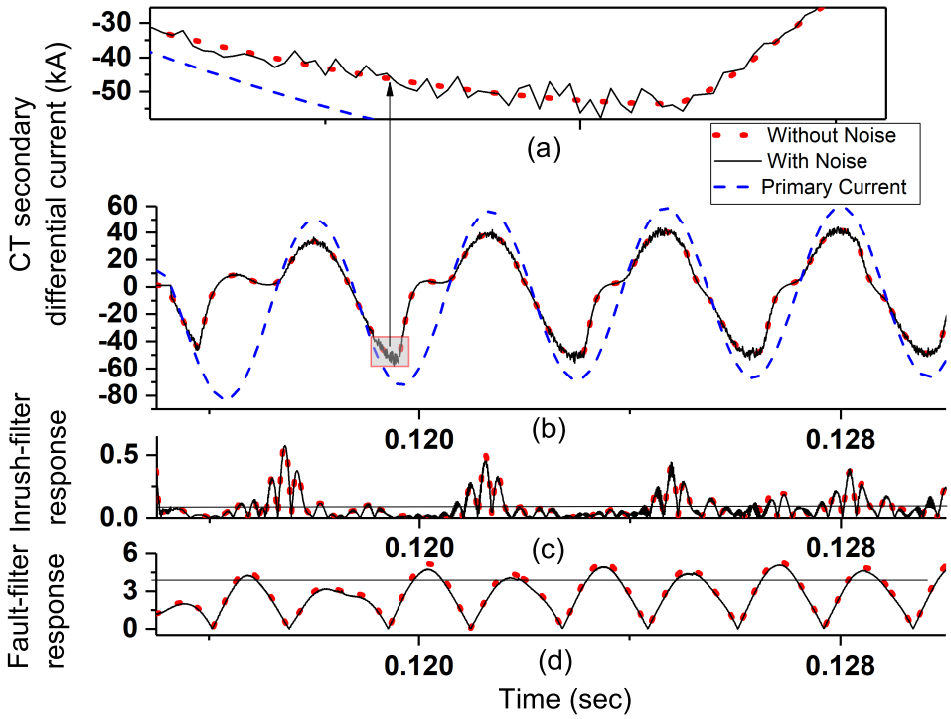

Figure 3.38: Case of inter-turn fault current at 60% of winding and its noisy version for 315 MVA transformer, angle of inception 0° (a) Zoomed portion of CT secondary differential current (b) CT primary and CT secondary differential current (c) Response of inrush-filter (d) Response of fault-filter

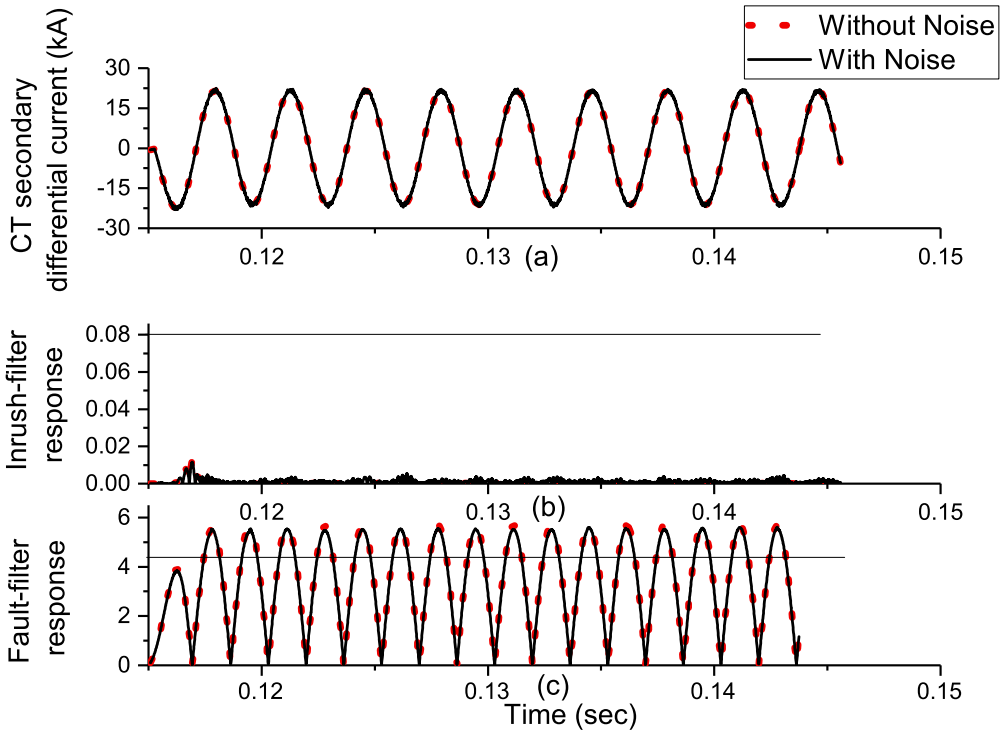

Figure 3.39: Case of inter-turn fault current at 20% of winding and its noisy version for 315 MVA transformer, angle of inception 0° (a) Zoomed portion of CT secondary differential current (b) CT primary and CT secondary differential current (c) Response of inrush-filter (d) Response of fault-filter

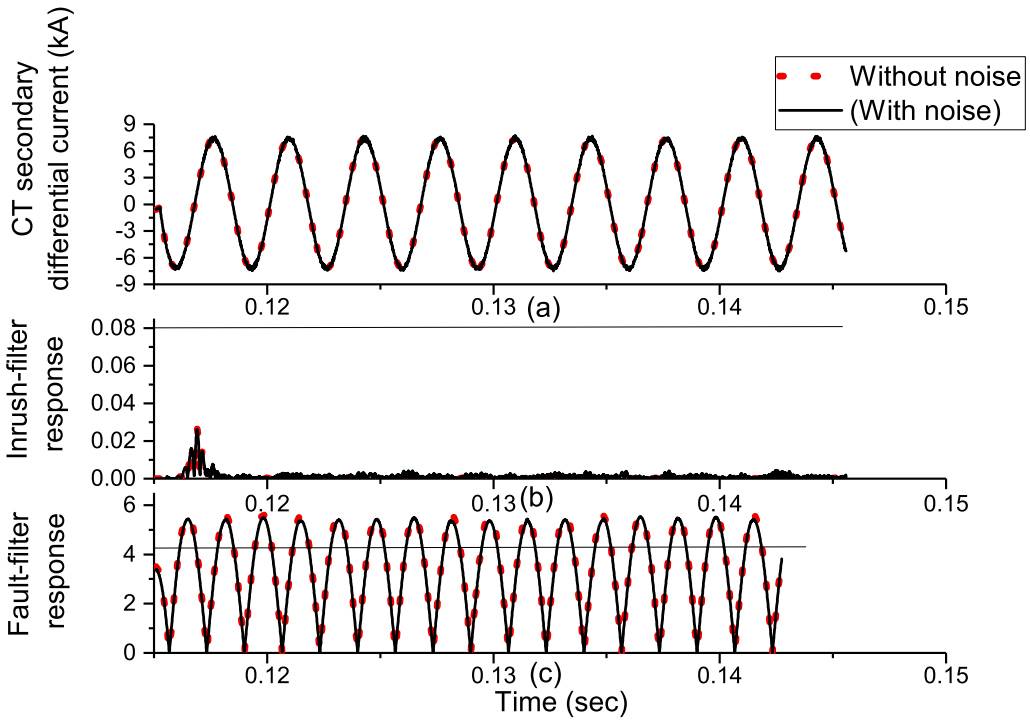

Figure 3.40: Case of inter-turn fault current at 10% of winding and its noisy version for 315 MVA transformer, angle of inception 0° (a) Zoomed portion of CT secondary differential current (b) CT primary and CT secondary differential current (c) Response of inrush-filter (d) Response of fault-filter

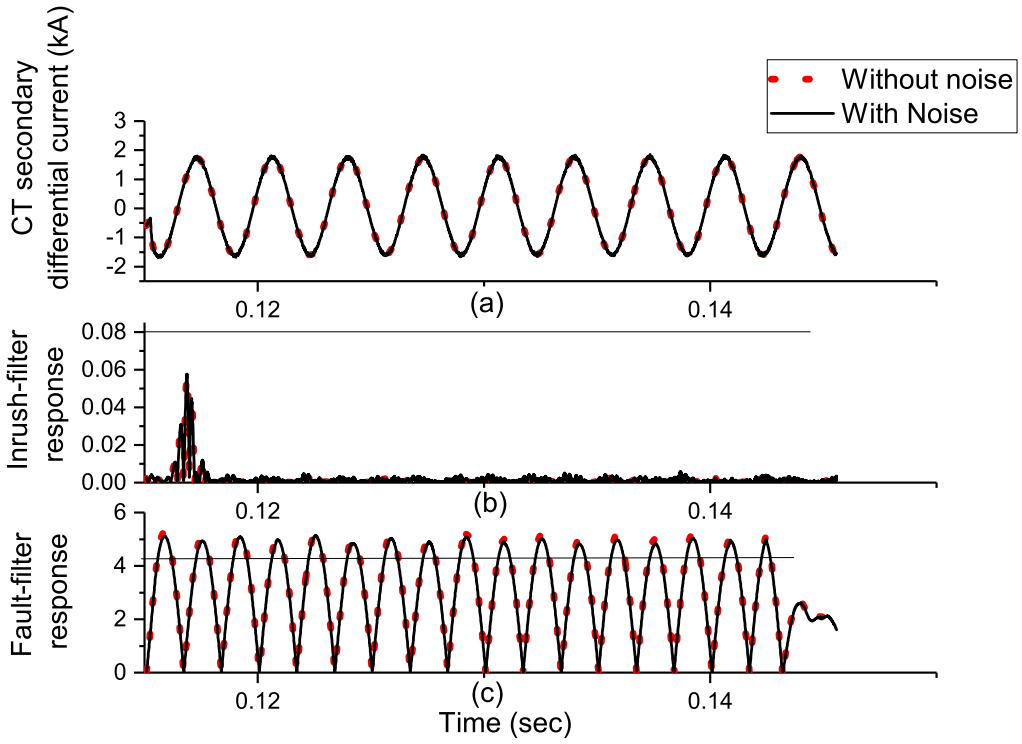

Figure 3.41: Case of inter-turn fault current at 5% of winding and its noisy version for 315 MVA transformer, angle of inception 0° (a) Zoomed portion of CT secondary differential current (b) CT primary and CT secondary differential current (c) Response of inrush-filter (d) Response of fault-filter

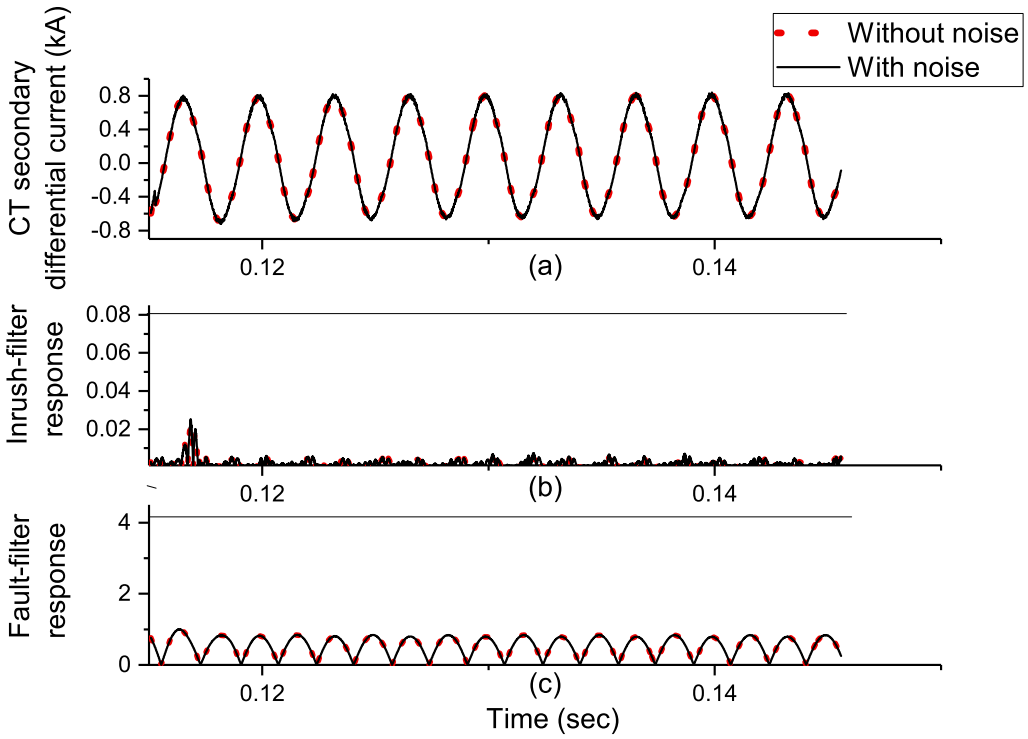

Figure 3.42: Case of inter-turn fault current at 2% of winding and its noisy version for 315 MVA transformer, angle of inception 0° (a) Zoomed portion of CT secondary differential current (b) CT primary and CT secondary differential current (c) Response of inrush-filter (d) Response of fault-filter

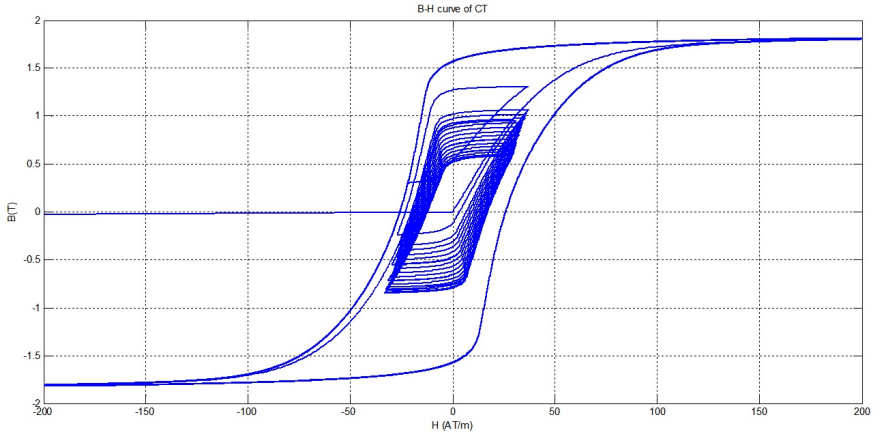

Figure 3.43: B-H curve

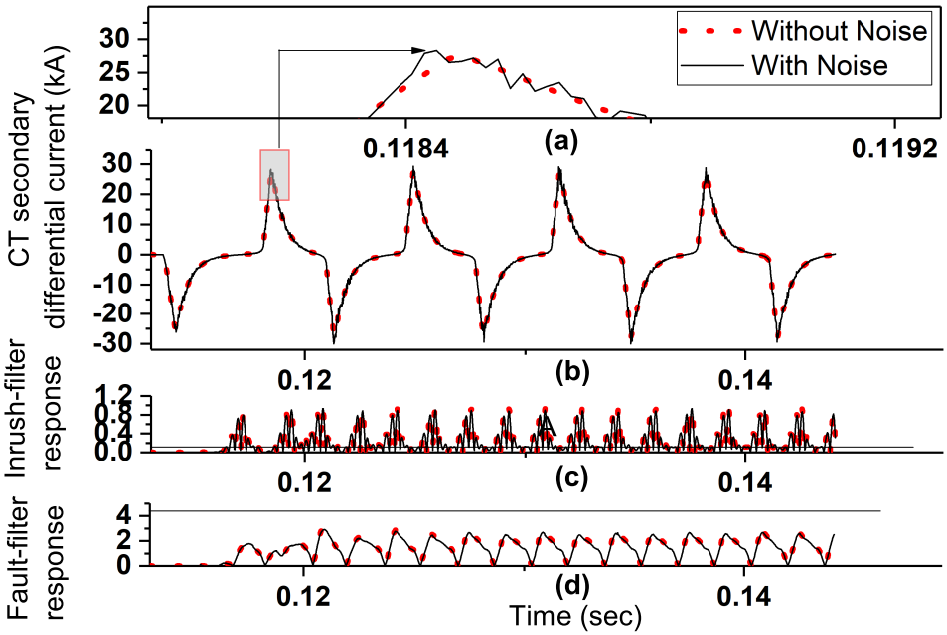

Figure 3.44: Case of in-zone fault current where detection fails due to poor CT (CT under high saturation) and its noisy version for 315 MVA transformer, angle of inception 0° (a) Zoomed portion of poor CT secondary differential current (b) CT secondary differential current (c) Response of inrush-filter (d) Response of fault-filter

fault waveform independent of inrush is reported for the first time through this work. The independent detection of fault and inrush waveform was made possible through the use of filters designed on the basis of matched fault wavelet and inrush wavelet respectively. The optimal matched wavelets developed are tested for *Inrush Processing* and *Fault Processing*.

The various operating conditions such as magnetizing inrush, over fluxing, sympathetic inrush, internal/in-zone faults, external faults and inter-turn faults of transformer are discussed in this chapter. CT saturation effects has strong impact on waveforms of these operating conditions. The analysis for CT saturation is presented in the chapter. The proposed differential protection scheme is tested on different waveforms obtained at different switching angles ranging from 0 to 180 degrees under various operating conditions including CT saturation effects. To test the generality of the scheme the testing waveforms are taken from MATLAB and PSCAD/EMTDC models. Transformer with rating 25 MVA is designed on MATLAB platform. Transformer with ratings 315 MVA and 200 MVA are designed on PSCAD/EMTDC platform. Also, the robustness against noise of the proposed scheme is evaluated by adding $\pm 5\%$ uniformly distributed noise to the obtained waveforms. The proposed scheme successfully detects and discriminate between the inrush and fault signals. It was observed that, for the cases considered, the cycles required to detect a *L-L fault* is 0.1 cycle, where as, to detect the sympathetic inrush the system can take up to 0.153 cycle. This situation suggest that there could be practical scenarios where fault could be detected faster than the inrush. Thus, the idea of independent detection of fault and inrush is advantageous over the traditional scheme.